MCP Papers in Press. Published on May 22, 2014 as Manuscript M113.037085

Specific glycosylation of membrane proteins in epithelial ovarian cancer cell lines: glycan structures reflect gene expression and DNA methylation status

Merrina Anugraham[1*], Francis Jacob[2, 3*], Sheri Nixdorf[3], Arun Vijay Everest-Dass[1], Viola Heinzelmann-Schwarz[2, 3], Nicolle H. Packer[1]

Affiliations:

[1] Department of Chemistry & Biomolecular Sciences, Biomolecular Frontiers Research Centre, Faculty of Science, Macquarie University, NSW 2109, Sydney, Australia

[2]Gynaecological Research Group, Department of Biomedicine, Women's University Hospital Basel, University of Basel, Basel 4003, Switzerland

[3]Ovarian Cancer Group, Adult Cancer Program, Lowy Cancer Research Centre, Prince of Wales Clinical School, University of New South Wales, NSW 2052, Sydney, Australia

*These authors contributed equally

This article contains supplemental tables **(ST1-2)** and figures **(SF1 - SF5)**

To whom all correspondence should be addressed: Professor Nicolle. H. Packer, Building E8C, Room 307, Department of Chemistry and Biomolecular Sciences, Macquarie University, New South Wales, 2109, Australia. Tel: +61-2-9850 8176; Fax: +61-2-9850 8313; E-mail: nicki.packer@mq.edu.au

Running Title: Alteration of membrane protein glycosylation in ovarian cancer

Keywords: serous ovarian cancer, glycosylation, mass spectrometry, glycomics, epigenetic regulation

Abbreviations: 5-Aza, 5-aza-2'-deoxycytidine; Gal, galactosamine; Man, mannose; Glc, glucose; Fuc, fucose; GlcNAc, *N*-acetyl-glucosamine; LacdiNAc, *N*,*N*'-diacetyl-lactosamine*;* GalNAc, *N*-acetyl-galactosamine; Neu5Ac, *N*-acetyl-neuraminic acid; LC, liquid chromatography; ESI, electrospray ionization; BPC, base peak chromatogram; EIC, extracted ion chromatogram; PGC, porous graphitized carbon; FIGO, International Federation of Gynaecology and Obstetrics; MIQE, Minimum Information for Publication of Quantitative Real-Time PCR Experiments.

Summary

Epithelial ovarian cancer is the fifth most common cause of cancer in women worldwide bearing the highest mortality rate among all gynaecological cancers. Cell membrane glycans mediate various cellular processes such as cell signalling and become altered during carcinogenesis. The extent to which glycosylation changes are influenced by aberrant regulation of gene expression is nearly unknown for ovarian cancer and remains crucial in understanding the development and progression of this disease. To address this effect, we analyzed the membrane glycosylation of non-cancerous ovarian surface epithelial (HOSE 6.3 and HOSE 17.1) and serous ovarian cancer cell lines (SKOV 3, IGROV1, A2780 and OVCAR 3), the most common histotype among epithelial ovarian cancers. *N*-glycans were released from membrane glycoproteins by PNG*ase* F and analyzed using nano-liquid chromatography on porous graphitized carbon and negative-ion electrospray ionization mass spectrometry (ESI-MS). Glycan structures were characterized based on their molecular masses and tandem MS fragmentation patterns. We identified characteristic glycan features that were unique to the ovarian cancer membrane proteins, namely the 'bisecting *N*-acetyl-glucosamine' type *N*-glycans, increased levels of α 2-6 sialylated *N*-glycans and '*N*,*N*'-diacetyl-lactosamine' (LacdiNAc) type *N*-glycans. These *N*-glycan changes were verified by examining gene transcript levels of the enzymes specific for their synthesis (*MGAT3*, *ST6GAL1* and *B4GALNT3*) using qRT-PCR. We further evaluated the potential epigenetic influence on *MGAT3* expression by treating the cell lines with 5-azacytidine, a DNA methylation inhibitor. For the first time, we provide evidence that *MGAT3* expression may be epigenetically regulated by DNA hypomethylation, leading to the synthesis of the unique 'bisecting GlcNAc' type *N*-glycans on the membrane proteins of ovarian cancer cells. Linking the observation of specific *N*-glycan substructures and their complex association with epigenetic programming of their associated synthetic enzymes in ovarian cancer could potentially be used for the development of novel anti-glycan drug targets and clinical diagnostic tools.

Introduction

Ovarian cancer is the fifth most common cause of cancer in women worldwide with the highest mortality rate among all gynaecological cancers (1). Most patients are often diagnosed when the disease has already metastasized to distant sites, resulting in a poor 5-year survival rate of 15-30 % when diagnosed at the advanced FIGO stages III–IV (2, 3). This poor prognosis is primarily attributed to difficulties in detecting the disease at an early stage, lack of noticeable early symptoms and inadequate screening methods. The most widely used clinical tumour marker for the diagnosis and management of this disease is CA125, a membrane-associated glycoprotein. However, its limited sensitivity and specificity impede the detection of early stage ovarian cancers (4-6).

Cellular glycosylation is a highly organized process in which the addition and modification of sugar or glycan residues on proteins and lipids are regulated by a large network of glycosyltransferases and glycosidases that are present in all tissues and cell types (7). The field of glycomics (study of glycans and glycan modifications) holds considerable promise as studies have begun to unravel the role of glycosylation in cancer (8-10). Upon malignant transformation, some of the enzymes in the glycosylation pathways are altered in their expression or activity and are thought to be associated with critical aspects of tumour development and metastasis. For example, β 1-6-*N*-acetyl-glucosaminyltransferase (GnT-V) which is responsible for the expression of tri- or tetra-antennary β 1-6-GlcNAc-bearing *N*-glycans on the cell surface and secreted glycoproteins, is often overexpressed in various cancers and has been correlated with higher invasive potential (11), metastasis (12), vascular remodeling (13) and tumour growth (14).

Recent developments in mass spectrometric methodologies and ionization techniques have also significantly improved over the last decade, thereby facilitating the structural analysis of glycans

(15, 16). Furthermore, the development of glyco-bioinformatics databases and tools such as UniCarb KB (17), GlycoMod (18), GlycoWorkBench (19), GlycReSoft (20), Multiglycan(21) have accelerated the pace of glycan characterization. In ovarian cancer, the majority of studies investigating *N*-glycans have been performed using serum (22-25), in which significant cancer-associated changes such as increased levels of branching of the *N*-glycans attached to glycoproteins (24) and increased sialylation of *N*-glycopeptides (25) have been found. As 90 % of ovarian cancers are of epithelial origin (26), an overview of the glycosylation landscape on cancer cell surface membrane glycoproteins is especially interesting as they have the potential to be used diagnostically, prognostically and therapeutically (27).

In this study, we examined specific *N*-glycan changes on glycoproteins from non-cancerous ovarian surface epithelial and ovarian cancer cell lines based on their membrane *N*-glycomic profiles. In addition, we performed a gene expression analysis of relevant glycosyltransferases and evaluated the potential epigenetic influence on glycosyltransferase-encoding genes to better understand their complex association with cell surface glycosylation. The link between aberrant glycosylation and epigenetics in cancer is an emerging area of research which still remains poorly understood (28, 29). Unlike irreversible genetic changes that affect the activity of these enzymes, epigenetic modifications can potentially be reversed by therapies such as de-methylation, which may be able to target defective glycosylation pathways to prevent metastasis in cancer (30). Hence, the specific glycan structural and synthetic alterations reported here serve as a preface towards understanding the key steps involved in the development and progression of ovarian cancer *via* the regulation of specific glycosyltransferases and the expression of their corresponding glycan structural epitopes.

Experimental Procedures

Materials

N-Glycosidase F (PNG*ase* F, recombinant clone derived from *Flavobacterium meningosepticum* and expressed in *Escherichia coli*) and protease inhibitor cocktail tablets were purchased from Roche Diagnostics (Basel, Switzerland). α 2-3 sialidase enzyme (Glyko® Sialidase S, recombinant derived from *Streptococcus pneumonia* and expressed in *Escherichia coli*) was purchased from Prozyme (Hayward, CA, USA). Immobilin-P Polyvinylidene Fluoride (PVDF, 0.2 µm) was obtained from Millipore (Billerica, MA, USA). Microtiter plates (Corning Costar® 96-well flat bottom) were purchased from Sigma Aldrich (St. Louis, MO, USA). Cation exchange resin beads (AG50W-X8) was obtained from BioRad (Hercules, CA, USA) and PerfectPure C18 Zip Tips were from Eppendorf (Hamburg, Germany). Mycoplasma detection kit VenorGeM® Mycoplasma Detection Kit was purchased from Minerva Biolabs GmbH (Berlin, Germany). RNA extraction NucleoSpin RNAII kit was obtained from Macherey & Nagel GmbH (Duren, Germany). Proteinase K was purchased from Finnzymes, ThermoFisher Scientific (Waltham, MA, USA). EZ DNA Methylation-Gold™ Kit for bisulfite conversion was from Zymo Research (Irvine, CA, USA). 5-aza-2'-deoxycytidine (5-Aza) and primers were purchased from Sigma Aldrich (St. Louis, MO, USA). Tris-hydrochloride (Tris-HCl), sodium chloride (NaCl), potassium hydroxide (KOH), ethylenediaminetetraacetic acid (EDTA), Triton X-114, polyvinyl polypyrrolidone 40 000 (PVP40) and sodium borohydride ($NaBH_4$) were obtained from Sigma Aldrich (St. Louis, MO, USA). Other reagents and solvents such as methanol, ethanol and acetonitrile were of HPLC or LC/MS grade.

Cell culture preparation

Serous ovarian cancer cell lines (SKOV 3, IGROV 1, A2780 and OVCAR 3) were from ATCC (Manassas, USA) and were cultured in RPMI 1640 medium, supplemented with 10 % foetal bovine serum. Normal, non-cancerous ovarian surface epithelial cell lines (HOSE 6.3 and HOSE 17.1) were obtained from the Garvan Research Institute (Sydney, Australia) and maintained in MCDB 105: Medium 199 (1:1, v/v) containing 10 % fetal bovine serum. All cells were grown to 70 % confluency at 37 ^{o}C in 5 % CO_2. Detailed characteristics of the non-cancerous and cancerous cell lines used in this study are listed in **Supplementary Table 1**. For extraction of genomic DNA and total RNA, cells were lysed directly after washing without harvesting by trypsinization. All cultures were free of mycoplasma, as determined by qualitative PCR using VenorGeM® Mycoplasma Detection Kit.

Cell membrane preparation and Triton X-114 phase partitioning of membrane proteins

Approximately 4 x 10^7 cells were washed twice with PBS and pelleted through centrifugation at 2, 500 x g for 20 mins to remove excess culture media. Cell pellets were re-suspended with 2 ml of lysis buffer (50 mM Tris-HCl, 100 mM NaCl, 1 mM EDTA and protease inhibitor at pH 7.4) and stored on ice for 20 mins. The cells were lysed using a Polytron homogenizer (Omni TH, Omni International Inc, VA) for 15 mins. Cellular debris and unlyzed cells were removed by centrifugation at 2, 000 x g for 20 mins at 4 ^{o}C. The supernatant was collected and diluted with 2 ml of Tris binding buffer (20 mM Tris-HCl, 100 mM NaCl at pH 7.4) and sedimented by ultracentrifugation at 120, 000 x g for 80 mins at 4 ^{o}C. The supernatant was discarded and 140 µl of Tris binding buffer was added into each sample to re-suspend the membrane pellet [modified from (31)]. A volume of 450 µl of Tris binding buffer containing 1 % (v/v) Triton X-114 was added to the suspended mixture, homogenized by pipetting and chilled on ice for 10 mins. Samples were heated at 37 ^{o}C for 20 mins and further subjected to phase partitioning by centrifugation at 200 x g for 3 mins. The upper aqueous layer was carefully removed and stored at -20 ^{o}C

until further analysis. The lower detergent layer containing the membrane proteins was mixed with 1 ml of ice-cold acetone and left overnight at -20 ^{o}C. Precipitated membrane proteins were pelleted by centrifugation at 1, 000 x g for 3 mins and solubilized in 10 µl of 8 M urea (31).

Enzymatic release of *N*-glycans from cell membrane proteins

N-glycans were prepared as previously described (32). Briefly, membrane proteins and glycoprotein standard (10 µg of fetuin) were spotted (2.5 µl x 4 times) onto a polyvinylidene difluoride (PVDF) membrane (Sequi Blot 0.2 µm, Millipore). The PVDF membrane was dried overnight at room temperature prior to staining and de-staining of the bound membrane proteins. The stained protein spots were cut and placed in separate wells of a 96-well microtiter plate and 100 µl of blocking buffer was added to each well. Upon removing the blocking buffer, the wells were then washed with MilliQ water and PNG*ase* F enzyme (2 µl of 1 U/µl PNG*ase* F and 8 µl of MilliQ water) was added to each well. A volume of 10 µl MilliQ water was added prior to an overnight incubation at 37 ^{o}C. The 96-well microtiter plate was sealed with parafilm to avoid sample evaporation. After sonication of the plate for 10 mins, approximately 20 µl of *N*-glycans were recovered from each well and combined with washings (50 µl of MilliQ water, twice) from the sample wells. To ensure a complete regeneration of the reducing terminus of the released *N*-glycans, 20 µl of 100 mM ammonium acetate (pH 5.0) was added to each sample (~120 µl) at room temperature for 1 h. After evaporation of the samples, the released *N*-glycans were reduced to alditols with 10 µl of 2 M $NaBH_4$ in 50 mM KOH and 10 µl of 50 mM KOH at 50 ^{o}C for 2 h and the reduction was quenched using 2 µl of glacial acetic acid.

Purification of *N*-glycan alditols derived from cell membrane proteins

The *N*-glycan alditols were desalted using cation exchange columns prepared in-house. Approximately 45 µl of cation exchange resin beads (AG50W-X8) were deposited onto reversed phase µ-C18 ZipTips (Perfect Pure, Millipore) placed in individual microfuge tubes. The tubes were then subjected to a brief spin followed by a series of individual pre-washing steps as described previously (32). Approximately 20 µl of *N*-glycan alditols were applied to the column, eluted with MilliQ water (50 µl, twice) and dried. Residual borate was removed by drying the samples under vacuum after the addition of methanol (100 µl, thrice). The purified *N*-glycan alditols were re-suspended in 15 µl of MilliQ water prior to mass spectrometry analysis.

LC-ESI-MS/MS of released *N*-glycan alditols

N-glycans were analyzed by nanoLC-MS/MS using an ion-trap mass spectrometer (LC/MSD Trap XCT Plus Series 1100, Agilent Technologies, USA) which was connected to an ESI source (Agilent 6330, USA). Samples were injected onto a Hypercarb porous graphitized carbon capillary column (5 µm Hypercarb KAPPA, 180 µm x 100 mm, Thermo Hypersil, Runcorn, UK) using an Agilent auto-sampler (Agilent 1100). The separation of *N*-glycans was carried out over a linear gradient of 0-45 % (v/v) acetonitrile /10 mM ammonium bicarbonate for 85 mins followed by a 10 min wash-step using 90 % (v/v) acetonitrile /10 mM ammonium bicarbonate at a flow rate of 2 µl/min. The sample injection volume was 7 µl and the MS spectra were obtained within the mass range of *m/z* 200–*m/z* 2200. The temperature of the transfer capillary was maintained at 300 ^{o}C and the capillary voltage was set at 3 kV. *N*-glycans were detected in the negative ionization mode as $[M-H]^-$ and $[M-2H]^{2-}$ ions. The MS data was analyzed and quantitated using Compass Data Analysis Version 4.0 software (Bruker Daltonics, USA. Monosaccharide compositions of the measured monoisotopic masses were determined using the GlycoMod tool (18) available on the ExPASy server (http://au.expasy.org/tools/glycomod) with a mass tolerance of ±0.5 Da).

The proposed glycan structures were manually assigned and interpreted from the tandem MS fragmentation spectra and further characterized with the GlycoWorkBench software tool (19). In addition, the web-based LC-MS/MS database, UniCarb KB (17), was also utilized to confirm fragmentation and retention time of *N*-glycans based on previously reported glycan structures that were available in the online library (33-36). The assignment of sialic acid linkages on the *N*-glycan structures were carried out through specific exoglycosidase treatment described below. Furthermore, *N*-glycans from fetuin were also used to confirm these linkages as previously described (37). Other structural features such as the 'bisecting GlcNAc' structures were characterized from diagnostic fragment ions previously described in negative ion mode fragmentation of *N*-glycans (38-40).

Data processing and statistical analysis of *N*-glycans

The MS ion intensity of each *N*-glycan composition was relatively quantified based on the peak areas of their extracted ion chromatogram (EIC) and expressed as a percentage of summed ion intensities for total *N*-glycans within each cell line. The glycan structures were classified into four major categories [high mannose/oligomannose, hybrid, complex (neutral and sialylated) and core fucosylated] based on the nomenclature proposed by Stanley *et. al*.(2009) (41). Following normalization to 100 %, the MS ion intensities were averaged for three replicates of each cell line and subjected to one-way analysis of variance (ANOVA) using SPSS Version 19.0 to assess their statistical significance at $p < 0.05$.

Specific α 2-3 sialidase digestion of *N*-glycan samples

To verify the sialic acid linkages, 5 µl *N*-glycans (~30 µg of membrane proteins) were digested with 2 µl of α 2-3 sialidase S (2 mU) in 2 µl of 5X reaction buffer and made up to 10 µl with water. The reaction mixture was vortexed and incubated at 37 ^{o}C overnight prior to LC-ESI-MS analysis. A matched untreated glycan sample (3 µl) was made up to 10 ul with water and used as a control for comparison.

Compositional monosaccharide analysis

Compositional analysis of monosaccharides was performed to verify the presence of the monosaccharide residue, *N*-acetyl-galactosamine, on the released *N*-glycans of the non-cancerous and cancerous cell lines. For neutral amino monosaccharides, 20 µl of released *N*-glycan alditols were hydrolyzed by treatment with 4 M HCl (100 µl of 8 M HCl in 80 µl MilliQ water) at 100 °C for 6 h. Hydrolyzed samples were evaporated to dryness and reconstituted in 50 µl of internal standard (0.1 M 2-deoxy-D-glucose). Monosaccharide content was determined using a high-performance anion-exchange chromatography with pulsed amperometric detection (HPAEC-PAD) system which comprised of the Bio-LC (Dionex, CA, USA) equipped with gradient pumps (GS50, Dionex) and a pulsed amperometric detector (ED50A, Dionex). 20 µl of amino monosaccharides were injected for each sample in duplicate and separated isocratically on a Dionex CarboPac™ PA–10 column (2×250 mm, Thermo Scientific) at a flow rate of 1.0 ml/min using 12 mM NaOH. Data was collected and analyzed using Chromeleon software (SP5 Build 1914, Dionex Version 6.70, Dionex Corporation).

Total RNA and genomic DNA extraction

In order to examine the potential gene expression of associated glycosyltransferases (n=17) and reference genes (n=3), non-cancerous ovarian surface epithelial and ovarian cancer cells were grown in 6-well plates (NUNC, Thermo Fisher Scientific, Roskilde, Denmark). Prior to cell lysis, cells were washed twice with PBS, and the cellular contents of two wells of a 6-well plate were combined. Total RNA extraction was performed using the NucleoSpin RNAII kit (Macherey-Nagel, Germany) according to the manufacturer's instructions. RNA was eluted in 50 µl of RN*ase* free water. Total RNA was measured at $A_{260/230\ nm}$ and $A_{260/280\ nm}$ using the NanoDrop ND-1000 spectrophotometer (Thermo Fisher Scientific, Denmark). RNA integrity was confirmed *via* an electropherogram (Agilent Bioanalyzer RNA 6000 Nano).

For genomic DNA extraction, the cellular contents of two wells of a 6-well plate were combined. Cells were lysed using 250 µl of lysis buffer (20 mM Tris-HCl, 4 mM Na_2EDTA and 100 mM NaCl) followed by the addition of 25 µl of 10 % (w/v) SDS. The lysed cell suspensions were vortexed vigorously and subsequent Proteinase K digestion (2.5 µl) was performed for a minimum of 2 h at 55 °C. Residual undigested proteins were precipitated using 200 µl of 5.3 M NaCl followed by 13, 000 x g centrifugation for 30 min at 4 °C. Supernatant was transferred to a new microfuge tube and an equal volume of ice-cold isopropanol was added. DNA was precipitated by inverting tubes several times. Precipitated DNA was washed with 70 % ethanol and dissolved in 10 mM of Tris-HCl at pH 8.5. DNA concentration was measured using spectrophotometry as described above for RNA.

Reverse transcription (RT) and quantitative PCR (qPCR)

Total RNA (1 µg) was reverse-transcribed using the iScript Reverse Transcription Supermix for RT-qPCR (Bio-Rad Laboratories, Australia) in a total volume of 20 µl according to the manufacturer's instructions. The complementary DNA (cDNA) was stored at -20 °C until further use. RT-qPCR was performed in concordance to MIQE guidelines (42). Reference genes were selected as previously described (43) and listed in **Table 2**. Target gene primers were designed by QuantPrime (44). Primer sequences were cross-checked using the web-based tool *in-silico* PCR (http://genome.ucsc.edu/cgi-bin/hgPcr) on the human genome browser at UCSC (45) against gene and genomic targets. RT-qPCR was performed on the Applied Biosystems 7500 Fast Real Time PCR system (Applied Biosystems, Switzerland) in 96-well microtitre plates for all six cell lines (SKOV 3, IGROV 1, A2780, OVCAR 3, HOSE 6.3 and HOSE 17.1). Optimal reaction conditions were obtained using 1x SensiFast™ SYBR with low ROX as the reference dye (Bioline, Biolabo, Switzerland), 400 nM specific sense, 400 nM specific antisense primer, RN*ase*/DN*ase*-free water, and cDNA template in a final reaction volume of 10 µl. Amplifications were performed starting with a 30 sec enzyme activation at 95 °C, followed by 40 cycles of denaturation at 95 °C for

5 sec, and then annealing/extension at 60 °C for 30 sec. At the end of each run, a melting curve analysis was performed between 65-95 °C. All samples and negative controls were amplified in triplicates and the mean value obtained was then used for further analysis.

To compare the RNA transcript levels of 6 cell lines for 10 targeted genes, cycle of quantification (Cq) values were generated directly at a specific threshold. The fluorescence signals obtained at a defined RNA concentration were plotted and linear regression was performed to identify the best linear relationship representing the standard curve. The slope of the linear equation was applied to calculate the efficiency according to the equation, $E = (10^{[-1/slope]}-1) \times 100$. Raw data, including the melting and amplification curves, generated by the ABI 7500 software Version 2.0.6. (Applied Biosystems, Switzerland) were analysed. Raw data were extracted and further data analysis was performed using the R statistical programming language Version 2.15.1 (http://CRAN.R-project.org).

5-aza-2'-deoxycytidine treatment

To investigate the potential influence of DNA methylation on *MGAT3* and *ST6GAL1* expression, the DNA methyltransferase inhibitor 5-aza-2'-deoxycytidine (5-Aza) was applied to all cell lines as follows: 10^5 cells were seeded in 6-well plates (NUNC, Thermo Fisher Scientific, Roskilde, Denmark) and incubated at 37 °C for 24 h. Culture medium was removed every 24 h and replaced by new medium containing 2.5 µM 5-Aza in 50 % (v/v) acetic acid. Samples were harvested after 24 h, 48 h and 72 h of treatment. Total RNA was extracted as described above. Mock control cells were treated with 50 % (v/v) acetic acid at a dilution identical to that of 5-Aza treated cells. The histone deacetylase inhibitor trichostatin A (TSA) was used as additional control (to exclude involvement of histone methylation) in which cells were treated with 5.0 µM TSA.

Results

To identify specific membrane *N*-glycan changes in serous ovarian cancer cell lines (SKOV 3, IGROV 1, A2780 and OVCAR 3) and non-cancerous ovarian surface epithelial cell lines (HOSE 6.3 and HOSE 17.1) (46), global glycosylation profiles of the glycans released from total membrane proteins by PNG*ase* F were acquired using mass spectrometry. The glycan structures were assigned based on manual interpretation of the tandem MS fragment spectra.

Relative quantitation of *N*-glycans of membrane proteins from non-cancerous and cancerous cell lines

The LC-ESI-MS/MS glycomic profiles were compared between the 2 non-cancerous and 4 cancerous cell lines to identify specific *N*-glycan alterations in terms of compositional and structural features. The major difference in structures between the *N*-glycans on membrane proteins from non-cancerous and cancerous cell lines are indicated in the representative glycomic profiles of one non-cancerous (HOSE 6.3) and one ovarian cancer (SKOV 3) cell line **(Figure 1).**

In total, 53 individual *N*-glycan masses (including structural and compositional isomers) were detected across all six cell lines of which 33 *N*-glycan masses were present in all the non-cancerous and cancerous cell lines **(Table 1)**. In order to determine if there were quantitative differences between these glycans in the membrane proteins of the non-cancerous and cancerous cell lines, the common *N*-glycans present in both non-cancerous and cancerous cell lines were statistically analyzed based on their *N*-glycan classes [high mannose, hybrid, complex (neutral and sialylated) and core fucosylated]. As shown in **Figure 2**, we observed significantly higher ($p < 0.05$) levels of high mannose *N*-glycans in the cancerous cell lines as compared to the non-cancerous cell lines with correspondingly lower levels of complex neutral ($p < 0.0001$) and complex sialylated *N*-glycans ($p < 0.05$) observed in ovarian cancer when compared to non-cancerous cell lines. Similarly, core fucosylated *N*-glycans were also found to be significantly lower ($p <$

0.01) in ovarian cancer cell lines as compared to the non-cancerous cell lines. No significant differences were observed in the overall expression of *N*-glycans in the total hybrid *N*-glycan subgroup. *O*-glycosylation was also investigated by reductive beta-elimination release from the membrane proteins of all the mentioned cell lines (non- cancer and cancerous) followed by PGC LC MS/MS. Less than five structures consisting of Core 1 and Core 2 *O*-glycans were found and there were no significant changes in the relative intensities of these structures between the non-cancer and cancer cell lines. Hence, the regulation of *O*-glycosylation was not further investigated.

α 2-6 sialylation

Upon performing a one-way ANOVA analysis to determine quantitative differences between the non-cancerous and cancerous cell lines, each *N*-glycan subgroup was examined for qualitative differences arising due to the presence of specific structural isomers. Porous graphitized carbon (PGC) LC-ESI-MS enables the separation of isomers of differently linked sialylated *N*-glycans based on their corresponding retention times **(Figure 3)**. Both the complex and hybrid sialylated *N*-glycan subgroups were found to contain isomeric glycan structures pertaining to differences in α 2-6 or α 2-3 linked sialylation.

For example, the monosialylated biantennary complex *N*-glycan with *m/z* $[1038.9]^{2-}$ detected in the cancer cell line, IGROV 1 **[Figure 3A(i)]** consists of the monosaccharide composition $(Neu5Ac)_1(Hex)_2$ $(HexNAc)_2(dHex)_1$ +$(Man)_3(GlcNAc)_2$ and comprises of two isomers; namely a sialylated, core fucosylated biantennary *N*-glycan with the Neu5Ac (sialic acid) linked either by a α 2-6 or α 2-3 linkage to the terminal Gal residue located on either arm. Sialylated isomers can be distinguished based on retention time differences as previously described (37, 39, 47) with the α 2-3 linked isomers having a stronger affinity to PGC and thereby eluting later as compared to the α 2-6 linked sialylated glycans. For the above *N*-glycan isomers, the α 2-6 linked sialic acid glycan isomers were shown to elute from the porous graphitized carbon column approximately 7-8 minutes earlier than the α 2-3 linked glycan isomers. The

linkages were orthogonally verified using α 2-3 sialidase that resulted in the loss of the late eluting *N*-glycan peaks bearing the α 2-3-linked sialic acid **[Figure 3A(ii)]**. This α 2-6 monosialylated fucosylated biantennary complex *N*-glycan (*m/z* $[1038.9]^{2-}$) and the corresponding monosialylated, non-fucoslyated structure of *m/z* $[965.9]^{2-}$ $[(Neu5Ac)_1(Hex)_2\ (HexNAc)_2 + (Man)_3(GlcNAc)_2]$ was observed only in the ovarian cancer cells **(Supplementary Figure 1A and 1B)**. The disialylated biantennary complex *N*-glycan with *m/z* $[1184.5]^{2-}$ $[(Neu5Ac)_2(Hex)_2(HexNAc)_2\ (dHex)_1 + (Man)_3(GlcNAc)_2]$ **(Supplementary Figure 1C)** was also present with additional isomers in the ovarian cancer cells. As represented in **Figure 3B(i) and (ii),** the extracted ion chromatograms (EIC) of *N*-glycans in the hybrid category also revealed the presence of additional isomers of the α 2-6 monosialylated *N*-glycan isomers with *m/z* $[864.3]^{2-}$ $[(Neu5Ac)_1(Hex)_2\ (HexNAc)_1 + (Man)_3(GlcNAc)_2]$, *m/z* $[945.3]^{2-}$ $[(Neu5Ac)_1(Hex)_3\ (HexNAc)_1 + (Man)_3(GlcNAc)_2]$ and *m/z* $[937.3]^{2}$ $[(Neu5Ac)_1\ (Hex)_2\ (HexNAc)_1(dHex)_1 + (Man)_3(GlcNAc)_2]$ in all ovarian cancer cell lines but not in the non-cancerous cells.

Bisecting GlcNAc

Apart from the 33 *N*-glycans common to all analysed cell lines, we identified 6 unique *N*-glycans (*m/z* $[840.8]^{2-}$, *m/z* $[913.9]^{2}$, *m/z* $[921.9]^{2-}$, *m/z* $[994.9]^{2-}$, m/z $[1177.5]^{2-}$ and m/z $[1140.5]^{2-}$) which were present on the cell membrane proteins of all four cancerous cell lines, but not on the non-cancerous cell lines (**Table 1; Supplementary Figure 2**). These *N*-glycans, representing approximately 5-13 % of total relative ion intensities of all four ovarian cancer cell lines **(Figure 2)** consisted of bi- and tri-antennary *N*-glycans which were found to have a bisecting GlcNAc (*N*-acetyl glucosamine) residue attached in a β 1-4 linkage to the innermost mannose of the *N*-glycan core. This linkage is catalyzed by the action of a specific enzyme, β 1-4-*N*-acetyl-glucosaminyltransferase III (GnT-III) encoded by the gene *MGAT3.* The structural assignment of the bisecting-type *N*-glycans was carried out based on the MS/MS fragmentation described by Harvey (48). In negative mode fragmentation spectra of *N*-glycans, the D ion

arises from the loss of the chitobiose core and the substituents forming the 3-antennae; thus the D ion mass corresponds to the composition of the 6-arm antenna as well as the two remaining branching core mannose residues. However, in bisecting type *N*-glycans, there is an additional loss of the β1-4 linked GlcNAc which results in the formation of the D-221 ion that is diagnostic for the presence of these structures. As observed in **Figure 4 (inset)**, the extracted ion chromatogram (EIC) of neutral bisecting GlcNAc *N*-glycan with *m/z* $[994.9]^{2-}$[$(Hex)_2(HexNAc)_3(dHex)_1$+$(Man)_3(GlcNAc)_2$] is seen only in the ovarian cancer cell lines **(Figure 4c-f).** When this parent ion mass was fragmented, the D-221 fragment ion mass at *m/z* $[670.3]^{1-}$ which corresponds to the composition, Gal-GlcNAc-Man-Man - loss of H_2O was observed in the MS/MS spectra of all five bisecting type *N*-glycan structures as shown in **Supplementary Figure 3A-E.** An example of another the diagnostic D-221 fragment ion at *m/z* $[508.3]^{1-}$ corresponding to GlcNAc-Man-Man - loss of H_2O, was also observed in the MS/MS spectrum for the *N*-glycan with *m/z* $[913.9]^{2-}$(**Supplementary Figure 3F)**.

LacdiNAc-type *N*-glycans

Several *N*-glycans specific to only the cell membrane proteins of SKOV 3 and IGROV 1 cell lines were also detected at low intensities, in which their monosaccharide compositions were predicted to contain a mixture of fucosylated, di-fucosylated and sialylated LacdiNAc motifs **(Table 1)**. We identified 4 *N*-glycans (m/z $[913.9]^{2-}$, m/z $[934.4]^{2-}$, m/z $[1059.4]^{2-}$, m/z $[1205.0]^{2-}$) that were present in both the cell lines (**Supplementary Figure 4)** while the remaining 6 *N*-glycans (m/z $[905.9]^{2-}$, m/z $[986.9]^{2}$, m/z $[1007.4]^{2-}$, m/z $[1059.9]^{2-}$, m/z $[1080.5]^{2-}$ and m/z $[1132.4]^{2-}$), consisted of mono and di- fucosylated LacdiNAc motifs which were present only in the IGROV 1 cell line (**Supplementary Figure 5)**. The representative MS/MS fragmentation ion spectra of LacdiNAc-type *N*-glycan (m/z $[934.4]^{2-}$) as well as the fucosylated (m/z $[1080.5]^{2-}$) and sialylated (m/z $[1205.0]^{2-}$) LacdiNAc derivatives are shown in **Figure 5**. The MS/MS fragmentation spectra, although at low intensities, contained adequate fragment ions

corresponding to both glycosidic and cross ring cleavages to facilitate the identification of the LacdiNAc antennae on these *N*-glycans. As observed in **Figure 5A**, the fragmentation spectra of the parent ion at *m/z* $[934.4]^{2-}$[$(HexNAc)_4$ $(dHex)_1$+$(Man)_3(GlcNAc)_2$] contained a prominent cross ring cleavage ion arising from the non-reducing terminal end of the *N*-glycan structure. This ^{1,3}A cross-ring cleavage ion at m/z $[465.2]^{1-}$, also termed as F ion, has a composition of GalNAc - GlcNAc-O-CH=CH-O- (GalNAc + GlcNAc + 59^-) which comprises the LacdiNAc disaccharide and two carbon atoms of the branching Man residue. Another pair of diagnostic ions which occurred as glycosidic cleavages at the non-reducing end was also observed as B/Y ions (m/z $[405.2]^{1-}$ and m/z $[1463.6]^{1-}$), clearly providing a definitive identification of the LacdiNAc antennae. Similarly, other derivatives of the LacdiNAc motif such as the fucosylated LacdiNAc (GalNAc-(Fuc)GlcNAc) and sialylated LacdiNAc (Neu5Ac-GalNAc-GlcNAc) trisaccharides were also found to contain the B ion at *m/z* $[551.2]^{1-}$ and *m/z* $[696.3]^{1-}$ for the parent ion with m/z $[1080.5]^{2-}$ [$(HexNAc)_4$ $(dHex)_3$+$(Man)_3(GlcNAc)_2$] and m/z $[1205.0]^{2-}$[$(Neu5Ac)_2(Hex)_1(HexNAc)_3(dHex)_1$+ $(Man)_3$ $(GlcNAc)_2$] respectively (**Figure 5B and 5C**). The presence of the monosaccharide residue, *N*-acetyl-galactosamine (GalNAc) in the PNG*ase* F released *N*-glycans was also verified through compositional monosaccharide analysis which revealed trace amounts of GalNAc in the IGROV 1 cell line which was not detected in the other non-cancerous and cancerous cell lines (**Supplementary Table 2**).

Gene expression of specific glycosyltransferases in ovarian cancer cell lines

The detection of α 2-6 sialylation and bisecting GlcNAc in the *N*-glycans of all of the four ovarian cancer cell lines as compared to the non-cancerous cell lines may be attributed to the regulation of specific enzymes within the glycosylation pathway, specifically the α 2-6 sialylatransferase (*ST6GAL 1* gene) and the bisecting GlcNAc transferase (*MGAT 3* gene*)*. Similarly, the identification of the LacdiNAc-type *N*-glycans, despite their low intensities, in two of the four ovarian cancer cell lines also warranted the investigation of specific gene expression of the various β 1-3/4 *N*-acetyl-galactosaminyltransferases

(*B3GALNT* and *B4GALNT* genes). To determine this, the relative transcript abundance of these genes was investigated in the two non-cancerous and four cancerous cell lines. In addition, we also profiled five *ST3Gal* sialyltransferases (*ST3GAL 1-5*) to determine the corresponding expression of enzymes responsible for the *N*-glycans bearing α 2-3 linked sialic acid residues, and six α 1-2/3/4/6 fucosyltransferases (FUT2-5,8,9) which corresponded to *N*-glycans bearing either core and/or terminal fucosylation. According to MIQE guidelines, RNA integrity was based on the RNA integrity number (RIN) of which obtained values of $A_{260/280}$ (2.08-2.10), $A_{260/230}$ (1.95-2.21) and ratio 28s/18s (2.0-2.3) indicated purified and intact total RNA extracts. Each glycosyltransferase encoding gene (n=17) and three reference genes (*HSPCB*, *SDHA* and *YWHAZ*) were examined for qPCR assay performance on at least three 10-fold dilutions, ranging from a minimum of 50 pg to a maximum of 100 ng of initial total RNA. PCR efficiency was detected as being the lowest in *ST3GAL1* (83.3%) and the highest in *FUT5* (120.5%). The coefficient of determination (R^2) was always ≥ 0.910 **(Table 2)**. The remaining candidate genes for this study, namely the α 1-3 fucosyltransferase 6 (*FUT6*), α 1-3 fucosyltransferase 7 (*FUT7*) and β 1-4 *N*-acetyl-galactosaminyltransferase 4 (*B4GALNT4*) did not reveal reliable qPCR performance due to non-detectable expression of mRNA transcripts in all investigated cell lines (n=6) and were therefore excluded from this study.

The ΔCq of each 'glyco-gene' (normalized against the logarithmic mean of reference genes) was applied by visualizing and clustering 'glyco-gene' expression among the tested cell lines **(Figure 6A)**. The expression of *ST6GAL1* ($p < 0.001$), *MGAT3* ($p < 0.001$) and *B4GALNT3* ($p = 0.015$) were significantly decreased in the non-cancerous cell lines as compared to the high expression observed in the ovarian cancer cell lines. In contrast, the non-cancerous cell lines showed significantly increased expression of *ST3GAL5* compared to all ovarian cancer cell lines ($p = 0.026$). *ST3GAL4* was abundantly expressed in both non-cancerous and ovarian cancer cell lines as compared to *ST3GAL3* which had varying transcript

levels. The investigation of fucosyltransferase encoding genes did not reveal any differential gene expression for core fucosylation (*FUT8*) and terminal fucosylation (*FUT2*, *4* and *5*) between the non-cancerous and ovarian cancer cell lines, although a significant increase in gene expression for *FUT3* and *FUT9* was observed specifically in the OVCAR 3 cell line as compared to the other cell lines.

We used both the data on the *N*-glycan structures containing bisecting GlcNAc and α 2-6/ α 2-3 sialylation as detected by LC-ESI-MS and the corresponding gene expression of the selected glycosyltransferases (*MGAT3*, *ST6GAL1* and *ST3GAL5*) to investigate their potential correlation **(Figure 6B)**. This was achieved by calculating the total relative ion intensities for the bisecting GlcNAc *N*-glycans (n=6 structures) and α 2-6/ α 2-3 sialylated *N*-glycans (n=11 structures) respectively, expressing them as a percentage of the total relative ion intensities of all *N*-glycans from each cell line and plotting these percentage values against the ΔCq of the corresponding glycosyltransferases. The linear dependence (R^2) obtained revealed a strong correlation between bisecting GlcNAc and *MGAT3* expression (r = 0.79) and between α 2-6 sialylation and *ST6GAL1* expression (r = 0.76) while moderately linear association was observed between α 2-3 sialylation and *ST3GAL5* expression (r = 0.66). These correlations emphasize that the specific changes in *N*-glycan structures seen between non-cancerous and cancerous cells can be directly attributable to the expression of the genes responsible for their synthesis. In particular, the bisecting GlcNAcylation and α 2-6 sialylation of the glycan structures expressed on the membrane proteins of ovarian cancer cells are directly correlated with the increased expression of the genes, *MGAT3* and *ST6GAL1*.

DNA hypermethylation and *MGAT3* expression

The exclusive presence of bisecting GlcNAc on *N*-glycans from all tested ovarian cancer cell lines highly correlated with *MGAT3* expression while the absence of bisecting GlcNAc in both non-cancerous cell lines was in full concordance with the reduced expression of *MGAT3*. In an attempt to understand the

molecular mechanism underlying the decreased *MGAT3* transcription in the non-cancerous cells, we investigated whether epigenetic dysregulation by hypermethylation might be responsible for silencing the *MGAT3* gene in the non-cancerous cells. We treated the non-cancerous and ovarian cancer cell lines with 5-aza-2'-deoxycytidine (5-Aza), an inhibitor of DNA methyltransferase, and tested for *MGAT3* expression. In addition, cells were treated with Trichostatin A (TSA), a selective inhibitor of class I and II histone deacetylases to exclude the potential alteration of *MGAT3* expression by histone epigenetic involvement. Within a 2 day-treatment period with 5-Aza, we observed a significant increase ($p < 0.05$) of *MGAT3* transcripts in non-cancerous cell lines as indicated by a relative *MGAT3* expression of up to 324-fold and 83-fold for HOSE 6.3 and HOSE 17.1, respectively **(Figure 7A).** The reconstituted *MGAT3* gene PCR product for both non-cancerous cell lines was also visualized by agarose gel electrophoresis **(Figure 7B).** No or slightly increased *MGAT3* transcript levels were observed in the serous ovarian cancer cell lines with 5-Aza treatment except for IGROV1 cells that showed a 6.3-fold increase. TSA treatment revealed similar *MGAT3* expression in HOSE 17.1, OVCAR3, A2780 and IGROV1 cell lines with only minor variations in HOSE 6-3 and SKOV3. These data suggest that inhibition of DNA methyltransferases by 5-Aza subsequently lead to DNA hypomethylation, thereby increasing *MGAT3* expression in the two non-cancerous cell lines.

Discussion

Post-translational modifications on proteins, such as glycosylation, offer researchers the possibility of exploring new potential biomarkers for early ovarian cancer detection and novel treatment options or therapies for this disease. The acquisition of structural information pertaining to membrane *N*-glycans is therefore important as it exposes new cell surface membrane glycan targets or modifications which represent key enzymatic changes that occur in cancer within the glycosylation machinery. It is becoming apparent that these glycan alterations are not necessarily the consequence of mutations and deletions at the DNA level of the respective glycosyltransferases, but may rather be due to epigenetic modifications to the DNA such as hyper- or hypomethylation which regulate variable gene expression (49). In this study, we identify specific *N*-glycan alterations on the cell surface membrane proteins of serous ovarian cancer cell lines that correlate with differential gene expression of the corresponding glycosyltransferase-encoded genes. We also show that the primary glycosyltransferase alteration is epigenetically regulated *via* DNA methylation.

A defining *N*-glycan structural feature unique to the ovarian cancer cell lines analyzed in this study was the presence of bisecting *N*-acetylglucosamine on several complex *N*-glycans, representing 5-13% of the total *N*-glycans across four ovarian cancer cell lines. To our knowledge, no study has investigated bisecting GlcNAc structures on membrane proteins of serous ovarian cancer and normal human ovarian epithelial cells using *nano*ESI-LC-MS/MS to directly identify the presence of this determinant without the use of monoclonal antibodies or lectins. In a previous study by Wong *et. al.* (2003), mono-fucosylated, bisecting GlcNAc *N*-glycans were identified on CA125 which was isolated by gel filtration from the conditioned media of the serous ovarian cancer cell line, OVCAR 3 (50). The authors confirmed the presence of bisecting GlcNAc using gas chromatography mass spectrometry (GC-MS) linkage analysis which identified a 3,4,6-linked Man residue of the *N*-glycan core, implying the presence of the 4-linked

bisecting GlcNAc. For the first time, we have demonstrated that the expression of bisecting GlcNAc on *N*-linked glycoproteins is correlated with the expression of the *MGAT3* gene that expresses the enzyme that adds this monosaccharide in a β 1-4 linkage to the core of the *N*-glycans. This is consistent with a previous study using mouse models (n=9) and human fresh frozen tissue samples (n=5), in which there was elevated mRNA expression of *MGAT3* in endometrioid ovarian cancer in both species types as compared to normal ovaries (51). The authors used the lectin, *phytohaemagglutinin E* (E-PHA), which has specificity towards binding to bisecting-type *N*-glycan determinants on glycoproteins. Positive staining for E-PHA was detected in normal controls and more than 2-fold increase of bisecting GlcNAc was detected in the ovarian cancer tissue samples (51). In our study, however, bisecting GlcNAc was completely absent in both non-cancerous cell lines and comprised up to 13 % of the *N*-glycans in the cancer cells. The quantitative difference in observation could be due to non-specific cross reactive binding of the lectin or the variation in glycosylation of proteins between cell lines and tissues.

Importantly, this study provides strong evidence that the bisecting GlcNAc *N*-linked structures on the membrane proteins of serous ovarian cancer cells are a consequence of DNA hypomethylation. The suppression of *MGAT3* in non-cancerous cell lines was shown to be, at least partly, due to epigenetic silencing by DNA hypermethylation as evidenced by the reconstitution of the *MGAT3* gene expression after 5-Aza treatment. The enzyme, GnT-III, encoded by the *MGAT3* gene, is thus responsible for producing bisecting-type *N*-glycans on the proteins of epithelial ovarian cancer cell lines. Bisecting GlcNAc addition has been thought to suppress metastasis by preventing the addition of branched-type complex *N*-glycans (52-54). This correlates strongly with our finding of an increased proportion of complex type *N*-glycans in the non-cancerous cells as compared to the serous ovarian cancer cells. A recent study demonstrated that *MGAT3* mediated E-cadherin *N*-glycosylation is involved in epithelial-mesenchymal transitions and their findings point to an involvement of DNA methylation as a regulatory

mechanism of *MGAT3* (55). This supports our finding that the expression of bisecting GlcNAc on the entire *N*-glycoproteome is indeed a result of DNA hypomethylation of *MGAT3* transcriptional regulatory elements in serous ovarian cancer cells. However, the precise DNA region of the *MGAT3* gene which is affected by the hypomethylation is still under investigation as our preliminary method optimization has been hampered by the high amount of CpG islands surrounding the gene. It is possible that there are other factors besides DNA hypomethylation of *MGAT3* that can also stimulate the expression of *MGAT3* in all four serous ovarian cancer cells, although histone methylation does not appear to be significantly involved. Apart from DNA methylation, nucleosome occupancy is another regulatory element, in which nucleosome positioning could potentially influence the gene activation of *MGAT3* and thus regulate *MGAT3* expression. Studies have shown that both these epigenetic mechanisms form a combinatorial epigenetic profile of a genomic locus and are becoming increasingly associated with cancer (56, 57).

The other difference in the glycosylation of the *N*-linked glycans on the ovarian cancer cell glycoproteins was the exclusive expression of α 2-6 linked sialic acids. Sialylation of *N*-glycans is an important modification in cellular glycosylation and alterations in sialyltransferase expression have been implicated in tumor progression and metastasis (58). The sialylation of *N*-glycans is determined by the concerted action of sialyltransferases which are classified into four families based on the specific linkage of the sialic acid residue transferred to the glycan substrate (59). The enzyme investigated in this study, *ST6GAL1*, terminally sialylates Galβ1-4GlcNAcβ motifs on *N*-glycans and the correlated over-expression of this gene in the serous ovarian cancer cells as compared to the non-cancerous cells is consistent with other findings reported for colorectal (60), breast (61), cervical (62), liver (63) and ovarian cancers (58). The presence of hybrid and complex *N*-glycans bearing α 2-6 sialylation in ovarian cancer cell lines is also in good agreement with another mass spectrometric-based analysis on the total serum glycome which revealed that α 2-6 sialylation of acute-phase glycoproteins in ovarian cancer patients' serum increased

proportionally as compared to α 2-3 sialylation (64). The functional role of *ST6GAL1*-mediated sialylation of membrane proteins is yet to be fully understood although it has been shown that α 2-6 sialylation of membrane-associated β_1 integrins in ovarian epithelial cells induces increased adhesion and invasive potential (65).

The contrasting prevalence of α 2-3 sialylation on membrane *N*-glycans in non-cancerous compared to ovarian cancer cells could be attributed to the overlapping enzyme specificities of the *ST3GAL* sialyltransferase family (66). Three of the five *ST3GAL* sialyltransferases (*ST3GAL3, ST3GAL4* and *ST3GAL5*) profiled in this study are known to sialylate the Galβ1-3/4GlcNAcβ motif on glycoproteins and glycolipids (67-69). The preferential expression of *ST3GAL4* over *ST3GAL3* in all six tested cell lines in this study is consistent with results from the previously mentioned study using normal and serous ovarian cancer tissues (58). It is also interesting to note that the expression of *ST3GAL5*, was significantly reduced in all four ovarian cancer cell lines. The enzyme has also been reported to act exclusively on Galβ1-4Glc-Cer motifs on glycolipids, giving rise to the synthesis of the α 2-3 sialylated ganglioside, GM_3 (70). Since our study was limited to the changes on the membrane *N*-glycoproteins, it will be worthwhile extending the scope of our analysis in the future to also investigate the differential expression of glycolipids in ovarian cancer.

Another exciting feature of this study is the presence of the '*N*,*N*'-diacetyl-lactosamine' (LacdiNAc) motif observed in some of the *N*-glycans of the ovarian cancer cell lines. This terminal modification, which also has been reported to occur as α 1-3-fucosylated (71, 72), 4-O-sulphated (73) or sialylated (74) derivatives, is less well understood as compared to the *N*-acetyl-lactosamine type antennae (LacNAc; Gal-GlcNAc). LacdiNAc-type *N*-glycans have been found on various mammalian glycoproteins such as the pituitary luteinizing hormone (75), glycodelin (76) and tenascin-R (77) as well as in other non-mammalian hosts such as the human parasite, *Schistosoma mansoni* (72). This disaccharide (GalNAcβ1-

4GlcNAc) is synthesized by the action of specific β4- GalNAc transferases, β4GalNAcT3 and β4GalNAcT4, which are differently expressed in various organs of the human body such as the stomach, colon, testes and ovaries (78, 79). Studies have shown that this motif is also present in some *N*-glycans of tumor-associated glycoproteins such as secreted tissue plasminogen activator from Bowes melanoma cells (80) and secreted ribonuclease I from pancreatic tumor cells (81). Interestingly, this motif has been previously described in ovarian cancer in which LacdiNAc-type *N*-glycans were identified in SKOV 3-derived recombinant human EPO and endogenous glycoproteins of SKOV 3 cell lines using positive mode MALDI-TOF-TOF mass spectrometry (82). In addition to the identification of LacdiNAc, as well as sialylated LacdiNAc motifs, on membrane proteins using negative mode mass spectrometry in our study, the exclusive presence of fucosylated LacdiNAc-type *N*-glycans and the corresponding increase in gene expression of B4GALNT3 in the IGROV 1 cell line appear to be of significant interest. This is particularly due to the mixed histological classification of the tumor (endometrioid and serous) from which this IGROV 1 cell line is derived as compared to the rest of the ovarian cancer cell lines which are mainly derived from serous type tumours. This observation, together with the recent findings of fucosylated as well as sulphated LacdiNAcs in a clear cell ovarian cancer cell line, RMG-1 (73), further substantiates the need to explore the significance of this motif, not only as a possible biomarker but also to aid in the differentiation between various histological subtypes of ovarian cancer.

The high mannose structures observed to comprise a greater proportion of the protein *N*-glycans in all four ovarian cancer cell lines were the most abundant structures as compared to the other *N*-glycan subgroups. A similar study involving cytosolic glycoproteins from breast cancer cell lines also showed that high mannose *N*-glycans were significantly elevated in invasive and noninvasive breast cancer cells as compared to the normal breast epithelial cells (83). While it remains unclear whether high mannose glycans are a common feature of most cultured cell lines, the presence of high mannose structures

reported here correlates with the study by Jacob *et. al.* (2012) who showed that naturally occurring anti-glycan antibodies such as anti-Man, present in ovarian cancer patients' plasma exhibited specific binding of high mannose structures using a printed glycan-array technology (23). A recently developed monoclonal antibody, TM10, has also been shown to have specificity towards high mannose *N*-glycans on glycoproteins derived from human cancer cell lines, ranging from melanoma, prostate, breast and ovarian cancer cell lines including SKOV 3 (84). One particular study indicated that cancer cells derived from A431 human squamous carcinoma cell line displayed high-mannose EGFR precursors on their cell surface due to their incomplete processing in the Golgi apparatus (85). Hence, it is possible that the synthetic processing of the *N*-glycans by the addition of other sugar residues to form complex structures on the cell surface membrane glycoproteins appears to be inhibited in cancer cells and this, together with the presence of bisecting GlcNAc, may explain the relatively low proportion of complex neutral and sialylated *N*-glycans observed in our study for the ovarian cancer cells.

At present, ovarian cancer treatment options are limited to only cytoreductive surgery and platinum-based chemotherapy of which more than 80% of patients undergo relapse due to chemotherapy resistance [42]. Attempts aimed at prolonging the remission of this disease and improving survival rates must be intensified through the development of novel biomarkers or molecular drug targets (86). The cell lines selected for this study, particularly the non-cancerous human ovarian surface epithelial cells, are representative of the cell line models currently used for studying ovarian cancer (46). Despite their potential utility, factors such as cell culture conditions and established choice of media may contribute to underlying cellular differences that must be taken into consideration in any *in vitro*- based studies. The determination of specific structural and isomeric changes specific to ovarian cancer-associated membrane-derived *N*-glycans described in this study provides evidence for the potential of glycan candidates to detect and potentially treat ovarian cancer malignancy that must be further investigated

in vivo. Furthermore, we highlight the importance of epigenetic modifications, such as DNA methylation, in ovarian cancer that is now shown to be pivotal in understanding the complex interplay between cellular glycosylation and glycosyltransferase expression.

References

1. Jemal, A., Siegel, R., Xu, J., and Ward, E. (2010) Cancer statistics, 2010. *CA Cancer J Clin* 60, 277-300

2. Vathipadiekal, V., Saxena, D., Mok, S. C., Hauschka, P. V., Ozbun, L., and Birrer, M. J. (2012) Identification of a potential ovarian cancer stem cell gene expression profile from advanced stage papillary serous ovarian cancer. *PLoS One* 7, e29079

3. Berkenblit, A., and Cannistra, S. A. (2005) Advances in the management of epithelial ovarian cancer. *J Reprod Med* 50, 426-438

4. Sasaroli, D., Coukos, G., and Scholler, N. (2009) Beyond CA125: the coming of age of ovarian cancer biomarkers. Are we there yet? *Biomark Med* 3, 275-288

5. Meyer, T., and Rustin, G. J. (2000) Role of tumour markers in monitoring epithelial ovarian cancer. *Br J Cancer* 82, 1535-1538

6. Jacob, F., Meier, M., Caduff, R., Goldstein, D., Pochechueva, T., Hacker, N., Fink, D., and Heinzelmann-Schwarz, V. (2011) No benefit from combining HE4 and CA125 as ovarian tumor markers in a clinical setting. *Gynecol Oncol* 121, 487-491

7. Paulson, J. C., and Colley, K. J. (1989) Glycosyltransferases. Structure, localization, and control of cell type-specific glycosylation. *J Biol Chem* 264, 17615-17618

8. Taylor, A. D., Hancock, W. S., Hincapie, M., Taniguchi, N., and Hanash, S. M. (2009) Towards an integrated proteomic and glycomic approach to finding cancer biomarkers. *Genome Med* 1, 57

9. Dube, D. H., and Bertozzi, C. R. (2005) Glycans in cancer and inflammation--potential for therapeutics and diagnostics. *Nat Rev Drug Discov* 4, 477-488

10. Hakomori, S. (1996) Tumor malignancy defined by aberrant glycosylation and sphingo(glyco)lipid metabolism. *Cancer Res* 56, 5309-5318

11. Yamamoto, H., Swoger, J., Greene, S., Saito, T., Hurh, J., Sweeley, C., Leestma, J., Mkrdichian, E., Cerullo, L., Nishikawa, A., Ihara, Y., Taniguchi, N., and Moskal, J. R. (2000) Beta1,6-N-acetylglucosamine-bearing N-glycans in human gliomas: implications for a role in regulating invasivity. *Cancer Res* 60, 134-142

12. Couldrey, C., and Green, J. E. (2000) Metastases: the glycan connection. *Breast Cancer Res* 2, 321-323

13. Taniguchi, N., Ihara, S., Saito, T., Miyoshi, E., Ikeda, Y., and Honke, K. (2001) Implication of GnT-V in cancer metastasis: a glycomic approach for identification of a target protein and its unique function as an angiogenic cofactor. *Glycoconj J* 18, 859-865

14. Demetriou, M., Nabi, I. R., Coppolino, M., Dedhar, S., and Dennis, J. W. (1995) Reduced contact-inhibition and substratum adhesion in epithelial cells expressing GlcNAc-transferase V. *J Cell Biol* 130, 383-392

15. Mechref, Y., Hu, Y., Garcia, A., Zhou, S., Desantos-Garcia, J. L., and Hussein, A. (2012) Defining putative glycan cancer biomarkers by MS. *Bioanalysis* 4, 2457-2469

16. Harvey, D. J. (2000) Collision-induced fragmentation of underivatized N-linked carbohydrates ionized by electrospray. *J Mass Spectrom* 35, 1178-1190

17. Hayes, C. A., Karlsson, N. G., Struwe, W. B., Lisacek, F., Rudd, P. M., Packer, N. H., and Campbell, M. P. (2011) UniCarb-DB: a database resource for glycomic discovery. *Bioinformatics* 27, 1343-1344

18. Cooper, C. A., Gasteiger, E., and Packer, N. H. (2001) GlycoMod--a software tool for determining glycosylation compositions from mass spectrometric data. *Proteomics* 1, 340-349

19. Ceroni, A., Maass, K., Geyer, H., Geyer, R., Dell, A., and Haslam, S. M. (2008) GlycoWorkbench: a tool for the computer-assisted annotation of mass spectra of glycans. *Journal of proteome research* 7, 1650-1659

20. Maxwell, E., Tan, Y., Tan, Y., Hu, H., Benson, G., Aizikov, K., Conley, S., Staples, G. O., Slysz, G. W., Smith, R. D., and Zaia, J. (2012) GlycReSoft: a software package for automated recognition of glycans from LC/MS data. *PLoS One* 7, e45474

21. Yu, C. Y., Mayampurath, A., Hu, Y., Zhou, S., Mechref, Y., and Tang, H. (2013) Automated annotation and quantification of glycans using liquid chromatography-mass spectrometry. *Bioinformatics* 29, 1706-1707

22. Abbott, K. L., Lim, J. M., Wells, L., Benigno, B. B., McDonald, J. F., and Pierce, M. (2010) Identification of candidate biomarkers with cancer-specific glycosylation in the tissue and serum of endometrioid ovarian cancer patients by glycoproteomic analysis. *Proteomics* 10, 470-481

23. Jacob, F., Goldstein, D. R., Bovin, N. V., Pochechueva, T., Spengler, M., Caduff, R., Fink, D., Vuskovic, M. I., Huflejt, M. E., and Heinzelmann-Schwarz, V. (2012) Serum antiglycan antibody detection of nonmucinous ovarian cancers by using a printed glycan array. *Int J Cancer* 130, 138-146

24. Alley, W. R., Jr., Vasseur, J. A., Goetz, J. A., Svoboda, M., Mann, B. F., Matei, D. E., Menning, N., Hussein, A., Mechref, Y., and Novotny, M. V. (2012) N-linked glycan structures and their expressions change in the blood sera of ovarian cancer patients. *J Proteome Res* 11, 2282-2300

25. Shetty, V., Hafner, J., Shah, P., Nickens, Z., and Philip, R. (2012) Investigation of ovarian cancer associated sialylation changes in N-linked glycopeptides by quantitative proteomics. *Clin Proteomics* 9, 10

26. Colombo, N., Peiretti, M., Parma, G., Lapresa, M., Mancari, R., Carinelli, S., Sessa, C., Castiglione, M., and Group, E. G. W. (2010) Newly diagnosed and relapsed epithelial ovarian carcinoma: ESMO Clinical Practice Guidelines for diagnosis, treatment and follow-up. *Ann Oncol* 21 Suppl 5, v23-30

27. Schiess, R., Wollscheid, B., and Aebersold, R. (2009) Targeted proteomic strategy for clinical biomarker discovery. *Mol Oncol* 3, 33-44

28. Kim, Y. S., and Deng, G. (2008) Aberrant expression of carbohydrate antigens in cancer: the role of genetic and epigenetic regulation. *Gastroenterology* 135, 305-309

29. Zoldos, V., Horvat, T., Novokmet, M., Cuenin, C., Muzinic, A., Pucic, M., Huffman, J. E., Gornik, O., Polasek, O., Campbell, H., Hayward, C., Wright, A. F., Rudan, I., Owen, K., McCarthy, M. I., Herceg, Z., and Lauc, G. (2012) Epigenetic silencing of HNF1A associates with changes in the composition of the human plasma N-glycome. *Epigenetics* 7, 164-172

30. Saldova, R., Dempsey, E., Perez-Garay, M., Marino, K., Watson, J. A., Blanco-Fernandez, A., Struwe, W. B., Harvey, D. J., Madden, S. F., Peracaula, R., McCann, A., and Rudd, P. M. (2011) 5-AZA-2'-deoxycytidine induced demethylation influences N-glycosylation of secreted glycoproteins in ovarian cancer. *Epigenetics* 6, 1362-1372

31. Lee, A., Kolarich, D., Haynes, P. A., Jensen, P. H., Baker, M. S., and Packer, N. H. (2009) Rat liver membrane glycoproteome: enrichment by phase partitioning and glycoprotein capture. *J Proteome Res* 8, 770-781

32. Jensen, P. H., Karlsson, N. G., Kolarich, D., and Packer, N. H. (2012) Structural analysis of N- and O-glycans released from glycoproteins. *Nat Protoc* 7, 1299-1310

33. Estrella, R. P., Whitelock, J. M., Packer, N. H., and Karlsson, N. G. (2010) The glycosylation of human synovial lubricin: implications for its role in inflammation. *The Biochemical journal* 429, 359-367

34. Issa, S., Moran, A. P., Ustinov, S. N., Lin, J. H., Ligtenberg, A. J., and Karlsson, N. G. (2010) O-linked oligosaccharides from salivary agglutinin: Helicobacter pylori binding sialyl-Lewis x and Lewis b are terminating moieties on hyperfucosylated oligo-N-acetyllactosamine. *Glycobiology* 20, 1046-1057

35. Karlsson, N. G., and Thomsson, K. A. (2009) Salivary MUC7 is a major carrier of blood group I type O-linked oligosaccharides serving as the scaffold for sialyl Lewis x. *Glycobiology* 19, 288-300

36. Everest-Dass, A. V., Jin, D., Thaysen-Andersen, M., Nevalainen, H., Kolarich, D., and Packer, N. H. (2012) Comparative structural analysis of the glycosylation of salivary and buccal cell proteins: innate protection against infection by C. albicans. *Glycobiology*

37. Nakano, M., Saldanha, R., Gobel, A., Kavallaris, M., and Packer, N. H. (2011) Identification of glycan structure alterations on cell membrane proteins in desoxyepothilone B resistant leukemia cells. *Mol Cell Proteomics* 10, M111 009001

38. Everest-Dass, A. V., Kolarich, D., Campbell, M. P., and Packer, N. H. (2013) Tandem mass spectra of glycan substructures enable the multistage mass spectrometric identification of determinants on oligosaccharides. *Rapid Commun Mass Spectrom* 27, 931-939

39. Everest-Dass, A. V., Abrahams, J. L., Kolarich, D., Packer, N. H., and Campbell, M. P. (2013) Structural feature ions for distinguishing N- and O-linked glycan isomers by LC-ESI-IT MS/MS. *J Am Soc Mass Spectrom* 24, 895-906

40. Harvey, D. J. (2005) Fragmentation of negative ions from carbohydrates: part 3. Fragmentation of hybrid and complex N-linked glycans. *J Am Soc Mass Spectrom* 16, 647-659

41. Stanley, P., Schachter, H., and Taniguchi, N. (2009) N-Glycans. In: Varki, A., Cummings, R. D., Esko, J. D., Freeze, H. H., Stanley, P., Bertozzi, C. R., Hart, G. W., and Etzler, M. E., eds. *Essentials of Glycobiology*, 2nd Ed., Cold Spring Harbor (NY)

42. Bustin, S. A., Benes, V., Garson, J. A., Hellemans, J., Huggett, J., Kubista, M., Mueller, R., Nolan, T., Pfaffl, M. W., Shipley, G. L., Vandesompele, J., and Wittwer, C. T. (2009) The MIQE guidelines: minimum information for publication of quantitative real-time PCR experiments. *Clin Chem* 55, 611-622

43. Jacob, F., Guertler, R., Naim, S., Nixdorf, S., Fedier, A., Hacker, N. F., and Heinzelmann-Schwarz, V. (2013) Careful Selection of Reference Genes Is Required for Reliable Performance of RT-qPCR in Human Normal and Cancer Cell Lines. *PLoS One* 8, e59180

44. Arvidsson, S., Kwasniewski, M., Riano-Pachon, D. M., and Mueller-Roeber, B. (2008) QuantPrime--a flexible tool for reliable high-throughput primer design for quantitative PCR. *BMC Bioinformatics* 9, 465

45. Kent, W. J., Sugnet, C. W., Furey, T. S., Roskin, K. M., Pringle, T. H., Zahler, A. M., and Haussler, D. (2002) The human genome browser at UCSC. *Genome Res* 12, 996-1006

46. Tsao, S. W., Mok, S. C., Fey, E. G., Fletcher, J. A., Wan, T. S., Chew, E. C., Muto, M. G., Knapp, R. C., and Berkowitz, R. S. (1995) Characterization of human ovarian surface epithelial cells immortalized by human papilloma viral oncogenes (HPV-E6E7 ORFs). *Exp Cell Res* 218, 499-507

47. Pabst, M., Bondili, J. S., Stadlmann, J., Mach, L., and Altmann, F. (2007) Mass + retention time = structure: a strategy for the analysis of N-glycans by carbon LC-ESI-MS and its application to fibrin N-glycans. *Anal Chem* 79, 5051-5057

48. Harvey, D. J., Crispin, M., Scanlan, C., Singer, B. B., Lucka, L., Chang, V. T., Radcliffe, C. M., Thobhani, S., Yuen, C. T., and Rudd, P. M. (2008) Differentiation between isomeric triantennary N-linked glycans by negative ion tandem mass spectrometry and confirmation of glycans containing galactose attached to the bisecting (beta1-4-GlcNAc) residue in N-glycans from IgG. *Rapid Commun Mass Spectrom* 22, 1047-1052

49. Rodriguez-Paredes, M., and Esteller, M. (2011) Cancer epigenetics reaches mainstream oncology. *Nat Med* 17, 330-339

50. Kui Wong, N., Easton, R. L., Panico, M., Sutton-Smith, M., Morrison, J. C., Lattanzio, F. A., Morris, H. R., Clark, G. F., Dell, A., and Patankar, M. S. (2003) Characterization of the oligosaccharides associated with the human ovarian tumor marker CA125. *J Biol Chem* 278, 28619-28634

51. Abbott, K. L., Nairn, A. V., Hall, E. M., Horton, M. B., McDonald, J. F., Moremen, K. W., Dinulescu, D. M., and Pierce, M. (2008) Focused glycomic analysis of the N-linked glycan biosynthetic pathway in ovarian cancer. *Proteomics* 8, 3210-3220

52. Schachter, H. (1986) Biosynthetic controls that determine the branching and microheterogeneity of protein-bound oligosaccharides. *Adv Exp Med Biol* 205, 53-85

53. Takahashi, M., Kuroki, Y., Ohtsubo, K., and Taniguchi, N. (2009) Core fucose and bisecting GlcNAc, the direct modifiers of the N-glycan core: their functions and target proteins. *Carbohydr Res* 344, 1387-1390

54. Lau, K. S., Partridge, E. A., Grigorian, A., Silvescu, C. I., Reinhold, V. N., Demetriou, M., and Dennis, J. W. (2007) Complex N-glycan number and degree of branching cooperate to regulate cell proliferation and differentiation. *Cell* 129, 123-134

55. Pinho, S. S., Oliveira, P., Cabral, J., Carvalho, S., Huntsman, D., Gartner, F., Seruca, R., Reis, C. A., and Oliveira, C. (2012) Loss and recovery of Mgat3 and GnT-III Mediated E-cadherin N-glycosylation is a mechanism involved in epithelial-mesenchymal-epithelial transitions. *PLoS One* 7, e33191

56. Wilson, B. G., and Roberts, C. W. (2011) SWI/SNF nucleosome remodellers and cancer. *Nat Rev Cancer* 11, 481-492

57. Kelly, T. K., Liu, Y., Lay, F. D., Liang, G., Berman, B. P., and Jones, P. A. (2012) Genome-wide mapping of nucleosome positioning and DNA methylation within individual DNA molecules. *Genome Res* 22, 2497-2506

58. Fwu, P. T., Wang, P. H., Tung, C. K., and Dong, C. Y. (2005) Effects of index-mismatch-induced spherical aberration in pump--probe microscopic image formation. *Appl Opt* 44, 4220-4227

59. Tsuji, S. (1996) Molecular cloning and functional analysis of sialyltransferases. *J Biochem* 120, 1-13

60. Dall'Olio, F., Chiricolo, M., and Lau, J. T. (1999) Differential expression of the hepatic transcript of beta-galactoside alpha2,6-sialyltransferase in human colon cancer cell lines. *Int J Cancer* 81, 243-247

61. Recchi, M. A., Hebbar, M., Hornez, L., Harduin-Lepers, A., Peyrat, J. P., and Delannoy, P. (1998) Multiplex reverse transcription polymerase chain reaction assessment of sialyltransferase expression in human breast cancer. *Cancer Res* 58, 4066-4070

62. Wang, P. H., Lee, W. L., Lee, Y. R., Juang, C. M., Chen, Y. J., Chao, H. T., Tsai, Y. C., and Yuan, C. C. (2003) Enhanced expression of alpha 2,6-sialyltransferase ST6Gal I in cervical squamous cell carcinoma. *Gynecol Oncol* 89, 395-401

63. Pousset, D., Piller, V., Bureaud, N., Monsigny, M., and Piller, F. (1997) Increased alpha2,6 sialylation of N-glycans in a transgenic mouse model of hepatocellular carcinoma. *Cancer Res* 57, 4249-4256

64. Saldova, R., Royle, L., Radcliffe, C. M., Abd Hamid, U. M., Evans, R., Arnold, J. N., Banks, R. E., Hutson, R., Harvey, D. J., Antrobus, R., Petrescu, S. M., Dwek, R. A., and Rudd, P. M. (2007) Ovarian cancer is associated with changes in glycosylation in both acute-phase proteins and IgG. *Glycobiology* 17, 1344-1356

65. Christie, D. R., Shaikh, F. M., Lucas, J. A. t., Lucas, J. A., 3rd, and Bellis, S. L. (2008) ST6Gal-I expression in ovarian cancer cells promotes an invasive phenotype by altering integrin glycosylation and function. *J Ovarian Res* 1, 3

66. Harduin-Lepers, A., Recchi, M. A., and Delannoy, P. (1995) 1994, the year of sialyltransferases. *Glycobiology* 5, 741-758

67. Kitagawa, H., and Paulson, J. C. (1993) Cloning and expression of human Gal beta 1,3(4)GlcNAc alpha 2,3-sialyltransferase. *Biochem Biophys Res Commun* 194, 375-382

68. Kitagawa, H., and Paulson, J. C. (1994) Cloning of a novel alpha 2,3-sialyltransferase that sialylates glycoprotein and glycolipid carbohydrate groups. *J Biol Chem* 269, 1394-1401

69. Ishii, A., Ohta, M., Watanabe, Y., Matsuda, K., Ishiyama, K., Sakoe, K., Nakamura, M., Inokuchi, J., Sanai, Y., and Saito, M. (1998) Expression cloning and functional characterization of human cDNA for ganglioside GM3 synthase. *J Biol Chem* 273, 31652-31655

70. Harduin-Lepers, A., Mollicone, R., Delannoy, P., and Oriol, R. (2005) The animal sialyltransferases and sialyltransferase-related genes: a phylogenetic approach. *Glycobiology* 15, 805-817

71. Kawar, Z. S., Haslam, S. M., Morris, H. R., Dell, A., and Cummings, R. D. (2005) Novel poly-GalNAcbeta1-4GlcNAc (LacdiNAc) and fucosylated poly-LacdiNAc N-glycans from mammalian cells expressing beta1,4-N-acetylgalactosaminyltransferase and alpha1,3-fucosyltransferase. *J Biol Chem* 280, 12810-12819

72. Wuhrer, M., Koeleman, C. A., Deelder, A. M., and Hokke, C. H. (2006) Repeats of LacdiNAc and fucosylated LacdiNAc on N-glycans of the human parasite Schistosoma mansoni. *FEBS J* 273, 347-361

73. Yu, S. Y., Chang, L. Y., Cheng, C. W., Chou, C. C., Fukuda, M. N., and Khoo, K. H. (2013) Priming mass spectrometry-based sulfoglycomic mapping for identification of terminal sulfated lacdiNAc glycotope. *Glycoconj J* 30, 183-194

74. Saarinen, J., Welgus, H. G., Flizar, C. A., Kalkkinen, N., and Helin, J. (1999) N-glycan structures of matrix metalloproteinase-1 derived from human fibroblasts and from HT-1080 fibrosarcoma cells. *Eur J Biochem* 259, 829-840

75. Smith, P. L., and Baenziger, J. U. (1992) Molecular basis of recognition by the glycoprotein hormone-specific N-acetylgalactosamine-transferase. *Proc Natl Acad Sci U S A* 89, 329-333

76. Dell, A., Morris, H. R., Easton, R. L., Panico, M., Patankar, M., Oehniger, S., Koistinen, R., Koistinen, H., Seppala, M., and Clark, G. F. (1995) Structural analysis of the oligosaccharides derived from glycodelin, a human glycoprotein with potent immunosuppressive and contraceptive activities. *J Biol Chem* 270, 24116-24126

77. Woodworth, A., Fiete, D., and Baenziger, J. U. (2002) Spatial and temporal regulation of tenascin-R glycosylation in the cerebellum. *J Biol Chem* 277, 50941-50947

78. Sato, T., Gotoh, M., Kiyohara, K., Kameyama, A., Kubota, T., Kikuchi, N., Ishizuka, Y., Iwasaki, H., Togayachi, A., Kudo, T., Ohkura, T., Nakanishi, H., and Narimatsu, H. (2003) Molecular cloning and characterization of a novel human beta 1,4-N-acetylgalactosaminyltransferase, beta 4GalNAc-T3,

responsible for the synthesis of N,N'-diacetyllactosediamine, galNAc beta 1-4GlcNAc. *J Biol Chem* 278, 47534-47544

79. Gotoh, M., Sato, T., Kiyohara, K., Kameyama, A., Kikuchi, N., Kwon, Y. D., Ishizuka, Y., Iwai, T., Nakanishi, H., and Narimatsu, H. (2004) Molecular cloning and characterization of beta1,4-N-acetylgalactosaminyltransferases IV synthesizing N,N'-diacetyllactosediamine. *FEBS Lett* 562, 134-140

80. Chan, A. L., Morris, H. R., Panico, M., Etienne, A. T., Rogers, M. E., Gaffney, P., Creighton-Kempsford, L., and Dell, A. (1991) A novel sialylated N-acetylgalactosamine-containing oligosaccharide is the major complex-type structure present in Bowes melanoma tissue plasminogen activator. *Glycobiology* 1, 173-185

81. Peracaula, R., Royle, L., Tabares, G., Mallorqui-Fernandez, G., Barrabes, S., Harvey, D. J., Dwek, R. A., Rudd, P. M., and de Llorens, R. (2003) Glycosylation of human pancreatic ribonuclease: differences between normal and tumor states. *Glycobiology* 13, 227-244

82. Machado, E., Kandzia, S., Carilho, R., Altevogt, P., Conradt, H. S., and Costa, J. (2011) N-Glycosylation of total cellular glycoproteins from the human ovarian carcinoma SKOV3 cell line and of recombinantly expressed human erythropoietin. *Glycobiology* 21, 376-386

83. Goetz, J. A., Mechref, Y., Kang, P., Jeng, M. H., and Novotny, M. V. (2009) Glycomic profiling of invasive and non-invasive breast cancer cells. *Glycoconj J* 26, 117-131

84. Newsom-Davis, T. E., Wang, D., Steinman, L., Chen, P. F., Wang, L. X., Simon, A. K., and Screaton, G. R. (2009) Enhanced immune recognition of cryptic glycan markers in human tumors. *Cancer Res* 69, 2018-2025

85. Johns, T. G., Mellman, I., Cartwright, G. A., Ritter, G., Old, L. J., Burgess, A. W., and Scott, A. M. (2005) The antitumor monoclonal antibody 806 recognizes a high-mannose form of the EGF receptor that reaches the cell surface when cells over-express the receptor. *FASEB J* 19, 780-782

86. Yap, T. A., Carden, C. P., and Kaye, S. B. (2009) Beyond chemotherapy: targeted therapies in ovarian cancer. *Nat Rev Cancer* 9, 167-181

Footnotes: Funding for this research was provided by the Macquarie University Postgraduate Research Scholarship and Northern Translational Cancer Research Grant No: 1470100 by NSW Cancer Institute, Australia (M.A.), NSW Cancer Institute Grant No: 09CRF202 (V.H.S.), Krebsliga Beider Basel (V.H.S), William Maxwell Trust (V.H.S.), Mary Elizabeth Courier Scholarship (V.H.S.) and Swiss National Foundation (F.J.).

Figure Legends

Table 1. Proposed *N*-glycan structures detected on the membrane proteins of non-cancerous and ovarian cancer cells. *N*-glycan structures released from non-cancerous and ovarian cancer cell membrane proteins were separated by PGC-LC-ESI and their structures were assigned based on MS/MS fragmentation (where possible), retention time differences and biological pathway constraints. Structures were depicted according to the CFG (Consortium of Functional Glycomics) notation with linkage placement to indicate linkages for sialic acid and fucose residues. Specific linkages corresponding Gal-GlcNAc (Type 1/Type 2) lactosamine linkages were not distinguished. *N*-glycan masses that were not structurally resolved and determined to consist of two or more isomer(s) are indicated with asterisks (*).Values represent mean ± SD of three separate experimental replicates.

Table 2. Established target gene primers and reference genes. Comprehensive list of primers used for quantitative RT-qPCR and parameters providing efficiency (E) and correlation coefficient (R^2) for each primer pair on target and reference genes applied in this study. Reference genes were established by Jacob *et al.* (2013) (43).

Fig.1. Representative glycomic profiles of *N*-glycans released from membrane proteins of HOSE 6.3 and SKOV 3 cell lines. An overview of the representative average MS *N*-glycan profiles in the range of *m/z* 600-1400 of the non-cancerous human ovarian surface epithelial (HOSE 6.3) and ovarian cancer cell line (SKOV 3) membrane glycoproteins (LC elution time: 30 to 70 mins). The *N*-glycan structures were identified by tandem MS and are represented mainly by the doubly charged species ion, *m/z* $[M\text{-}2H]^{2-}$. Singly charged $[M\text{-}H]^-$ ions with *m/z* 1235.0 and *m/z* 1397.5 are also shown in the figure. Number of isomers corresponding to structurally resolved mass ions is indicated in parentheses ( ). *N*-glycan masses that were not structurally resolved and determined to consist of two or more isomer(s) are indicated with asterisks (*).

Fig.2. Quantitation of relative abundances based on structural *N*-glycan type as shown in Table 1. Box plots indicating changes in the relative ion intensities of 33 common *N*-glycans (high mannose, hybrid, complex neutral, complex sialylated and core fucosylated) expressed in two non-cancerous human ovarian surface epithelial cells and four ovarian cancer cell lines. Levels of significant differences are indicated by respective *p*-values for all categories except for bisecting GlcNAc. Data represents the mean of three technical replicates.

Fig.3. Representative extracted ion chromatograms (EIC) of monosialylated *N*-glycans. (A) PGC- LC allows for the separation of α 2-6 and α 2-3 sialylated *N*-glycans based on retention time. The EICs obtained from the ovarian cancer cell line, IGROV 1 depict two major monosialylated *N*-glycans (with and without fucose), m/z $[965.9]^{2-}$ $[(Neu5Ac)_1(Hex)_2\ (HexNAc)_2+(Man)_3(GlcNAc)_2]$ and m/z $[1038.9]^{2-}$ $[(Neu5Ac)_1(Hex)_2(HexNAc)_2(dHex)_1+(Man)_3(GlcNAc)_2]$ which display α 2-3 and α 2-6 sialylated isomers at separate retention times (i). To orthogonally confirm the identity of the isomers containing α 2-6 linked sialic acids, released *N*-glycans from the membrane proteins of IGROV1 cells were treated with α 2-3-linked sialidase. The lower panel depicts the loss of the α 2-3 sialylated isomers for both *N*-glycans (ii).
(B) The EICs of three monosialylated hybrid *N*-glycans with *m/z* $[864.3]^{2-}$, *m/z* $[945.3]^{2-}$ and *m/z* $[937.3]^{2}$ are represented and the separate retention times for isomers with α 2-6-linked and α 2-3-linked sialic acid are illustrated in i) the non-cancerous epithelial cells (HOSE 6.3) and ii) ovarian cancer cell line (SKOV 3).

Fig.4. Example of a MS^2 fragment ion spectra depicting the diagnostic ions of bisecting GlcNAc type *N*-glycans in ovarian cancer cells. In *N*-glycans, the D-221 ion is formed when the bisecting GlcNAc attached to the innermost Man residue is cleaved from the 6-antenna comprising of HexNAc-bisecting GlcNAc-Man-Man. The fragment ion resulting from this specific cleavage of the bisecting bi-antennary *N*-glycan shown appears at *m/z* $[670.3]^{-}$. The insert to the right represents the extracted ion

chromatogram (EIC) of neutral bisecting GlcNAc *N*-glycan with *m/z* $[994.9]^{2-}$ $[(Hex)_2(HexNAc)_3\ (dHex)_1 +(Man)_3(GlcNAc)_2]$ in non-cancerous and ovarian cancer cell lines.

Fig.5. Representative MS^2 fragment ion spectra depicting the diagnostic ions for LacdiNAc type *N*-glycans in ovarian cancer cells. (A) Diagnostic ions characteristic for the identification of the HexNAc-HexNAc disaccharide, *m/z* $[405.2]^-$ and *m/z* $[465.2]^-$, are illustrated for the neutral bi-antennary core fucosylated *N*-glycan with *m/z* $[934.4]^{2--}$ $[(HexNAc)_4\ (dHex)_1+(Man)_3(GlcNAc)_2]$. Diagnostic ions which are characteristic for terminal fucosylated LacdiNAc (*m/z* $[551.2]^-$) and sialylated LacdiNAc ($[696.3]^-$) are illustrated for *N*-glycans with *m/z* $[1080.4]^{2-}$ $[(HexNAc)_4\ (dHex)_3+(Man)_3(GlcNAc)_2]$ (B) and $[1205.0]^{2-}$ $[(Neu5Ac)_2(Hex)_1(HexNAc)_3(dHex)_1+ (Man)_3\ (GlcNAc)_2]$ (C).

Fig.6. Quantitative RT-PCR of mRNA transcripts of glycosyltransferase genes and scatterplot analysis of glyco-gene expression (*MGAT3* and *ST6GAL1*) with corresponding *N*-glycan structures. Gene expression levels of glycosyltransferase mRNA transcripts (n=17) analyzed in two non-cancerous human ovarian surface epithelial cells (HOSE 6.3 and HOSE 17.1) and four ovarian cancer cell lines (SKOV 3, OVCAR 3, A2780 and IGROV 1). (A) Normalized (ΔCq) and clustered 'glyco gene' expression (row) among tested cell lines (column) visualized as heatmap. Dendrogram (row) shows clusters of correlating expression. Key at the right side indicates level of expression of transcripts from high (black) to low (white). Level of significant differences in transcript levels are indicated by asterisk (· $p < 0.1$; * $p < 0.05$; ** $p < 0.001$). Gene expression profiles of *MGAT3*, *ST6GAL1* and *ST3GAL5* show positive correlation with resulting glycan phenotype as illustrated by (B) scatterplots of *MGAT3*, *ST6GAL1* and *ST3GAL5* 'glyco gene' expression (abscissa) and their corresponding relative MS ion intensities of bisecting GlcNAc, α 2-6 and α 2-3 sialylated *N*-glycan structures (ordinate). Scatterplot data points circled in dashes represent two non-cancerous human ovarian surface epithelial cells and data points circled in dots represent four ovarian cancer cell lines used in this study. Data represents the mean of three technical replicates.

Fig.7. Evidence of *MGAT3* gene silencing by DNA hypermethylation in non-cancerous human ovarian surface epithelial cells. To determine if *MGAT3* gene expression is regulated epigenetically by DNA methylation, all cell lines were treated with 5-Aza, a DNA methylation inhibitor, and tested for *MGAT3* expression. (A) Heatmap illustration of *MGAT3* gene expression (ΔCq) normalized for all cell lines (abscissa) under different treatment conditions: no treatment (mock), Azacytidine (5-Aza), and Trichostatin A (TSA). In both non-cancerous cell lines, *MGAT3* gene expression was significantly increased after treatment with 5-Aza. Level of significant difference in transcript levels is indicated by asterisk (* $p < 0.05$). Transcription levels are based on 72 h treatment period. Key at the lower right side indicates level of *MGAT3* expression from high (black) to low (white). (B) Reconstituted *MGAT3* (by 5-Aza and mock treatment) and reference gene (*YWHAZ*) expression in normal ovarian surface epithelial cell lines are visualized by agarose gel electrophoresis.

Type	No	Glycan Mass $[M-H]^-$	$[M-2H]^{2-}$	Glycan Structures	Average Relative Intensity (n=3)					
					Non-Cancerous Cells		Ovarian Cancer Cells			
					HOSE 6.3	HOSE 17.1	SKOV 3	IGROV 1	A2780	OVCAR 3
High Mannose	1	1235.4	617.2	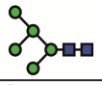	0.60 ± 0.15	0.63 ± 0.15	0.66 ± 0.04	0.62 ± 0.06	1.61 ± 0.06	1.79 ± 0.15
	2	1397.6	698.3	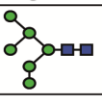	3.85 ± 0.78	2.89 ± 0.82	5.03 ± 1.37	7.91 ± 0.15	4.84 ± 0.54	3.97 ± 0.36
	3a	1559.6	779.3	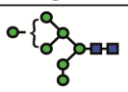	7.73 ± 0.51	4.40 ± 0.20	8.26 ± 0.15	11.30 ± 2.65	9.8 ± 2.20	6.72 ± 0.20
	3b	1559.6	779.3	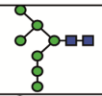	1.90 ± 0.96	1.8 ± 0.75	1.86 ± 0.35	2.15 ± 0.20	2.53 ± 0.25	2.18 ± 0.13
	4	1721.6	860.3	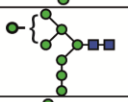	15.40 ± 1.76	13.97 ± 3.84	22.86 ± 7.60	16.00 ± 3.73	17.29 ± 3.40	14.96 ± 0.81
	5	1883.8	941.4	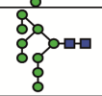	14.11 ± 0.92	14.06 ± 0.93	25.21 ± 0.85	24.57 ± 6.02	20.84 ± 0.06	19.29 ± 0.23
	6	2045.6	1022.3	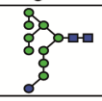	0.68 ± 0.11	0.58 ± 0.10	1.16 ± 0.14	1.43 ± 0.61	1.16 ± 0.21	1.18 ± 0.17
Hybrid	7	1260.5	-	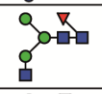	0.15 ± 0.07	0.01 ± 0.00	0.04 ± 0.00	0.01 ± 0.00	0.01 ± 0.00	0.01 ± 0.00
	8	1422.6	710.8	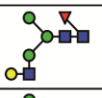	0.00	0.00	0.00	0.21 ± 0.10	0.00	0.00
	9a	1567.6	783.3	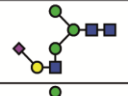	0.00	0.00	0.04 ± 0.00	0.08 ± 0.03	0.22 ± 0.03	0.01 ± 0.00
	9b	1567.6	783.3	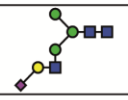	0.36 ± 0.12	0.31 ± 0.10	0.00	0.11 ± 0.05	0.17 ± 0.04	0.00
	10	1584.6	791.8	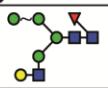	0.65 ± 0.14	0.56 ± 0.10	0.38 ± 0.13	0.34 ± 0.11	0.31 ±0.05	0.55 ± 0.03
	11	1600.6	799.8	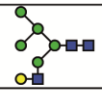	1.90 ± 0.36	1.44 ± 0.16	1.19 ± 0.54	1.04 ± 0.30	0.81 ± 0.11	2.21 ± 0.50
	12a	1713.6	856.3	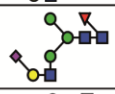	0.00	0.12 ± 0.20	0.32 ± 0.35	0.7 ± 0.21	2.21 ± 0.10	0.43 ± 0.20
	12b	1713.6	856.3	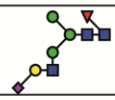	1.72 ± 0.27	0.85 ± 0.15	0.35 ± 0.12	1.06 ± 0.42	2.36 ± 0.20	0.54 ± 0.18
	13a	1729.6	864.3	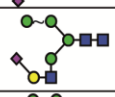	0.08 ± 0.25	0.02 ± 0.20	0.39 ± 0.25	0.38 ± 0.18	0.27 ± 0.05	0.99 ± 0.15
	13b	1729.6	864.3	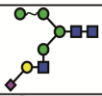	0.84 ± 0.40	0.80 ± 0.10	0.14 ± 0.20	0.30 ± 0.29	0.67 ± 0.06	0.38 ± 0.10
	14	1746.6	872.8		0.18 ± 0.08	0.28 ± 0.10	0.50 ± 0.08	0.20 ± 0.00	0.45 ± 0.04	0.72 ± 0.31

Type	No	Glycan Mass $[M-H]^-$	$[M-2H]^{2-}$	Glycan Structures	Average Relative Intensity (n=3)					
					Non-Cancerous Cells		Ovarian Cancer Cells			
					HOSE 6.3	HOSE 17.1	SKOV 3	IGROV 1	A2780	OVCAR 3
Hybrid	15a	1875.6	937.3		0.00	0.00	0.41 ± 0.16	0.20 ± 0.25	0.69 ± 0.16	0.62 ± 0.18
	15b	1875.6	937.3	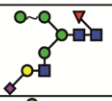	0.60 ± 0.06	0.36 ± 0.09	0.36 ± 0.12	0.41 ± 0.20	0.28 ± 0.14	0.60 ± 0.13
	16a	1891.6	945.3	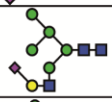	0.06 ± 0.19	0.06 ± 0.12	0.68 ± 0.04	0.47 ± 0.22	0.63 ± 0.12	1.43 ± 0.38
	16b	1891.6	945.3	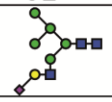	0.58 ± 0.10	0.42 ± 0.11	0.46 ± 0.03	0.43 ± 0.08	0.37 ± 0.03	0.7 ± 0.19
Complex Neutral	17	1463.6	731.2		0.59 ± 0.26	0.47 ± 0.06	0.90 ± 0.27	0.74 ± 0.03	0.76 ± 0.14	1.00 ± 0.17
	18	1625.6	812.3		1.63 ± 0.12	1.42 ± 0.19	0.76 ± 0.11	0.64 ± 0.14	1.40 ± 0.08	0.85 ± 0.35
	19	1641.6	820.3		4.65 ± 0.67	4.81 ± 0.76	0.87 ± 0.05	1.59 ± 0.62	0.91 ± 0.11	1.40 ± 0.24
	20	1666.4	832.8		0.28 ± 0.10	0.01 ± 0.00	1.31 ± 0.46	1.22 ± 0.40	0.77 ± 0.25	0.15 ± 0.05
	21	1682.6	840.8		0.00	0.00	0.30 ± 0.13	0.12 ± 0.05	0.70 ± 0.10	0.80 ± 0.16
	22	1771.8	885.4		0.47 ± 0.18	0.41 ± 0.04	0.00	0.00	0.00	0.00
	23	1787.6	893.3		14.43 ± 2.24	16.31 ± 2.81	3.14 ± 0.02	3.50 ± 0.22	3.81 ± 0.50	3.95 ± 0.91
	24	1812.8	905.9		0.00	0.00	0.00	0.24 ± 0.08	0.00	0.00
	25a	1828.8	913.9		0.00	0.00	0.12 ± 0.08	0.17 ± 0.13	1.70 ± 0.80	0.73 ± 0.18
	25b	1828.8	913.9	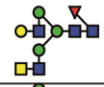	0.00	0.00	0.18 ± 0.04	0.49 ± 0.11	0.00	0.00
	26	1844.8	921.9	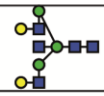	0.00	0.00	0.50 ± 0.09	1.37 ± 0.19	1.00 ± 0.13	1.60 ± 0.21
	27	1869.8	934.4	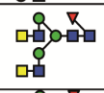	0.00	0.00	0.70 ± 0.30	0.51 ± 0.20	0.00	0.00
	28a	1933.6	966.3	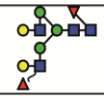	1.90 ± 0.90	3.57 ± 0.59	0.00	0.00	0.00	0.00
	28b	1933.6	966.3		0.48 ± 0.11	0.83 ± 0.20	0.00	0.00	0.00	0.00

Type	No	Glycan Mass $[M-H]^-$	$[M-2H]^{2-}$	Glycan Structures	Average Relative Intensity (n=3)					
					Non-Cancerous Cells		Ovarian Cancer Cells			
					HOSE 6.3	HOSE 17.1	SKOV 3	IGROV 1	A2780	OVCAR 3
Complex Neutral	29	1974.8	986.9	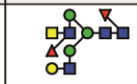	0.00	0.00	0.00	0.79 ± 0.28	0.00	0.00
	30	1990.8	994.9		0.00	0.00	2.60 ± 0.10	2.62 ± 0.60	3.77 ± 0.80	5.93 ± 1.06
	31	2006.8*	1002.9	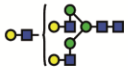	0.67 ± 0.25	1.14 ± 0.45	0.21 ± 0.07	0.31 ± 0.15	0.30 ± 0.12	0.27 ± 0.10
	32	2015.8	1007.4	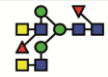	0.00	0.00	0.00	0.14 ± 0.06	0.00	0.00
	33	2079.8	1039.4	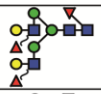	0.32 ± 0.08	0.65 ± 0.15	0.00	0.00	0.00	0.00
	34	2120.8	1059.9		0.00	0.00	0.00	0.56 ± 0.19	0.00	0.00
	35	2136.6	1067.8		0.00	0.00	0.00	0.31 ± 0.15	0.00	0.00
	36	2152.8*	1075.9	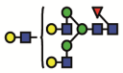	2.44 ± 0.65	3.44 ± 0.62	0.92 ± 0.19	1.18 ± 0.16	1.10 ± 0.34	1.25 ± 0.31
	37	2162	1080.5		0.00	0.00	0.00	0.39 ± 0.09	0.00	0.00
	38a	2356	1177.5	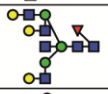	0.00	0.00	0.00	0.00	0.18 ± 0.15	1.40 ± 0.44
	38b	2356	1177.5	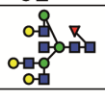	0.00	0.00	0.40 ± 0.07	0.23 ± 0.02	0.22 ± 0.11	0.00
	39	2518	1258.5	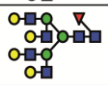	0.01 ± 0.00	0.60 ± 0.18	0.40 ± 0.15	0.37 ± 0.10	0.16 ± 0.05	0.53 ± 0.18
Complex Sialylated	40a	1916.6	957.8	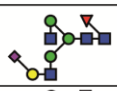	0.00	0.00	0.44 ± 0.00	0.07 ± 0.05	0.49 ± 0.03	0.58 ± 0.09
	40b	1916.6	957.8	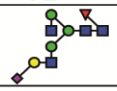	0.74 ± 0.17	0.81 ± 0.06	0.11 ± 0.05	0.14 ± 0.06	0.39 ± 0.07	0.40 ± 0.14
	41a	1932.8	965.9	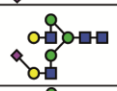	0.73 ± 1.20	0.79 ± 1.14	1.47 ± 0.36	1.38 ± 0.38	1.50 ± 0.26	2.09 ± 0.20
	41b	1932.8	965.9	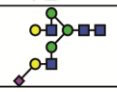	3.57 ± 1.11	5.44 ± 1.35	1.03 ± 0.27	1.86 ± 0.49	1.12 ± 0.47	1.13 ± 0.11
	42a	2078.8	1038.9		0.81 ± 0.43	1.00 ± 0.20	5.15 ± 1.20	1.91 ± 0.23	3.80 ± 0.09	7.72 ± 1.34
	42b	2078.8	1038.9	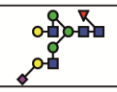	9.36 ± 0.75	9.12 ± 0.25	3.49 ± 2.18	3.23 ± 0.14	2.85 ± 0.10	1.41 ± 1.55

Type	No	Glycan Mass [M-H]$^-$	[M-2H]$^{2-}$	Glycan Structures	Average Relative Intensity (n=3)					
					Non-Cancerous Cells		Ovarian Cancer Cells			
					HOSE 6.3	HOSE 17.1	SKOV 3	IGROV 1	A2780	OVCAR 3
Complex Sialylated	43	2119.8*	1059.4	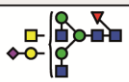	0.00	0.00	0.17 ± 0.12	0.36 ± 0.15	0.00	0.00
	44a	2223.8	1111.4		0.00	0.00	0.05 ± 0.10	0.10 ± 0.03	0.20 ± 0.50	0.27 ± 0.13
	44b	2223.8	1111.4	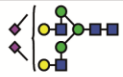	0.23 ± 0.19	0.11 ± 0.14	0.18 ± 0.11	0.13 ± 0.08	0.60 ± 0.41	0.35 ± 0.26
	44c	2223.8	1111.4	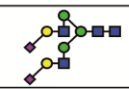	0.66 ± 0.20	0.86 ± 0.10	0.15 ± 0.15	0.18 ± 0.10	0.33 ± 0.12	0.52 ± 0.14
	45	2265.8*	1132.4		0.00	0.00	0.00	0.06 ± 0.02	0.00	0.00
	46a	2282.0	1140.5	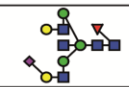	0.00	0.00	0.54 ± 0.06	0.35 ± 0.14	1.10 ± 0.14	2.80 ± 0.50
	46b	2282.0	1140.5	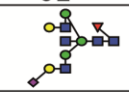	0.00	0.00	0.36 ± 0.17	0.30 ± 0.17	0.00	0.00
	47	2297.8*	1148.4	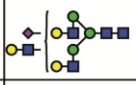	0.30 ± 0.00	0.53 ± 0.14	0.12 ± 0.02	0.23 ± 0.02	0.01 ± 0.00	0.01 ± 0.00
	48a	2370.0	1184.5	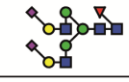	0.00	0.00	0.10 ± 0.19	0.42 ± 0.13	0.17 ± 0.19	0.12 ± 0.42
	48b	2370.0	1184.5	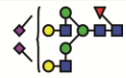	0.00	0.00	0.97 ± 0.30	0.38 ± 0.24	1.52 ± 0.20	0.35 ± 0.25
	48c	2370.0	1184.5	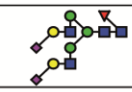	2.93 ± 0.76	2.32 ± 0.19	0.61 ± 0.21	0.53 ± 0.35	0.28 ± 0.31	1.60 ± 0.44
	49	2411.0	1205		0.00	0.00	0.03 ± 0.00	0.06 ± 0.02	0.00	0.00
	50	2444.0*	1221.5	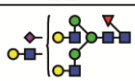	0.76 ± 0.40	1.31 ± 0.26	0.97 ± 0.30	0.65 ± 0.07	0.91 ± 0.15	1.12 ± 0.06
	51	2589.0*	1294.0	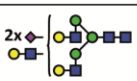	0.16 ± 0.05	0.17 ± 0.09	0.03 ± 0.00	0.03 ± 0.00	0.01 ± 0.00	0.01 ± 0.00
	52	2735.0*	1367.0	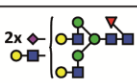	0.30 ± 0.14	0.23 ± 0.11	0.27 ± 0.09	0.03 ± 0.00	0.41 ± 0.13	0.37 ± 0.03
	53	3026.0*	1512.5	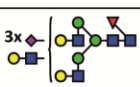	0.19 ± 0.10	0.09 ± 0.02	0.15 ± 0.10	0.19 ± 0.08	0.01 ± 0.00	0.01 ± 0.00

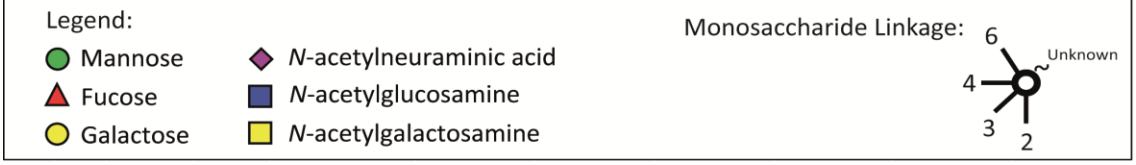

Table 1

Table 2

Symbol	Gene name	Acession number	Chromosmal location	Forward Primer 5‘-3‘	Reverse Primer 5‘-3	E in %	R^2
MGAT3	mannosyl (β-1,4-)-glycoprotein β-1,4-N-acetylglucosaminyl transferase	NM_002409.4	22q13.1	GGGATGAAGATGAGACGCTACAAG	AGGACAGGGTCTTGAAGAAGTGC	114.3	0.985
ST6GAL1	β-galactosamide α-2,6-sialyltranferase 1	NM_173217.2	3q27-q28b	CCATCCTCTGGGATGCTTGGTATC	ACGTCAGTCTTGCGCTTGGATG	102.9	0.991
ST3GAL1	β-galactoside α-2,3-sialyltransferase 1	NM_173344.2	8q24.22	AGTCACGACTTTGTCCTCAGGATG	TGGTCTTGGTCCCAACATCAGC	83.3	0.981
ST3GAL2	β-galactoside α-2,3-sialyltransferase 2	NM_006927.3	16q22.1	GCATGTGTGTGATGAGGTGAACG	TTCTCCCAGTAGTGGTGCCAGTTG	102.6	0.999
ST3GAL3	β-galactoside α-2,3-sialyltransferase 3	NM_174963	1p34.1	AGTGGCAGGACTTTAAGTGGTTG	AGAAGCCATCCGATGCACTCAC	91.4	0.963
ST3GAL4	β-galactoside α-2,3-sialyltransferase 4	NM_006278.2	11q24.2	CAGCCACGGAAGATTAAGCAGAAG	GCAATGTGCACCAAGTCACAGAG	111.8	0.999
ST3GAL5	β-galactoside α-2,3-sialyltransferase 5	NM_001042437.1	2p11.2	TGTGGACCCTGACCATGTAAAGAG	TGGCAAACTTGGGACGACATTCC	103.6	0.995
FUT2	α1-2 fucosyltransferase 2	NM_000511.5	19q13.3	TCACCGATGCTGGAAGGGTTTC	AACGACCAGCATGGCTTCTCTC	118.2	0.992
FUT3	α1-3/4 fucosyltransferase 3	NM_001097640.1	19p13.3	TCAGACAGGTCCAAGTTCAAGCC	TTACAGTCGATCCCACCTGTACCC	107.8	0.997
FUT4	α1-3 fucosyltransferase 4	NM_002033.3	11q21	TTTACCGAGGAAGGAGCCAAGG	GCTGGTTCTGCCACTGCTATTG	100.0	0.999
FUT5	α1-3 fucosyltransferase 5	NM_002034.2	19p13.3	TGCATCACTATGGGTGTGACCTC	TGAGGCATCGCAACACATCCAC	120.5	0.952
FUT8	α1-6 fucosyltransferase 8	NM_178155	14q24.3	GGCCTGTAAGTGAGACATGCAC	TTTGTCCTTCACTTCACCTGACC	89.4	0.998
FUT9	α1-3 fucosyltransferase 9	NM_006581.3	6q16	TGGCCTCATTAGCCACCTTCAG	TGGACAAGGATGGCATCTTCAGG	93.1	0.987
B4GALNT1	beta-1,4-N-acetyl-galactosaminyl transferase 1	NM_001478.3	12q13.3	GAGCCTTCAGGCAGCTTCT	CCTAGGGAGGCAGTCAGGTT	98.1	0.910
B4GALNT3	beta-1,4-N-acetyl-galactosaminyl transferase 3	NM_173593.3	12p13.33	TGGCATAGACCTCGTGAAGGAC	ACAGTGCTTCCGAATGGCATC	100.4	0.998
B3GALNT1	beta-1,3-N-acetyl-galactosaminyltransferase 1	NM_003781.3	3q25	TGCTCTATCACGTGGTGCTCTC	ACGCGAGCCGAAGGTTCTTTAC	116.8	0.997
B3GALNT2	beta-1,3-N-acetyl-galactosaminyltransferase 2	NM_152490.2	1q42.3	TGCCTTACTGAAGGAGGAAAGCAG	AGCTCGTTGTTTCCACAGTCCATC	106.3	0.986
HSPCB	Heat shock protein 90kDa alpha (cytosolic)	NM_007355	6p12	TCTGGGTATCGGAAAGCAAGCC	GTGCACTTCCTCAGGCATCTTG	103.1	0.998
YWHAZ	Tyrosine 3-monooxygenase/ tryptophan 5-monooxygenase activation protein, zeta polypeptide	NM_003406	8q23.1	ACTTTTGGTACATTGTGGCTTCAA	CCGCCAGGACAAACCAGTAT	101.2	0.998
SDHA	Succinate dehydrogenase complex, subunit A	NM_004168	5p15	TGGGAACAAGAGGGCATCTG	CCACCACTGCATCAAATTCATG	105.6	0.994

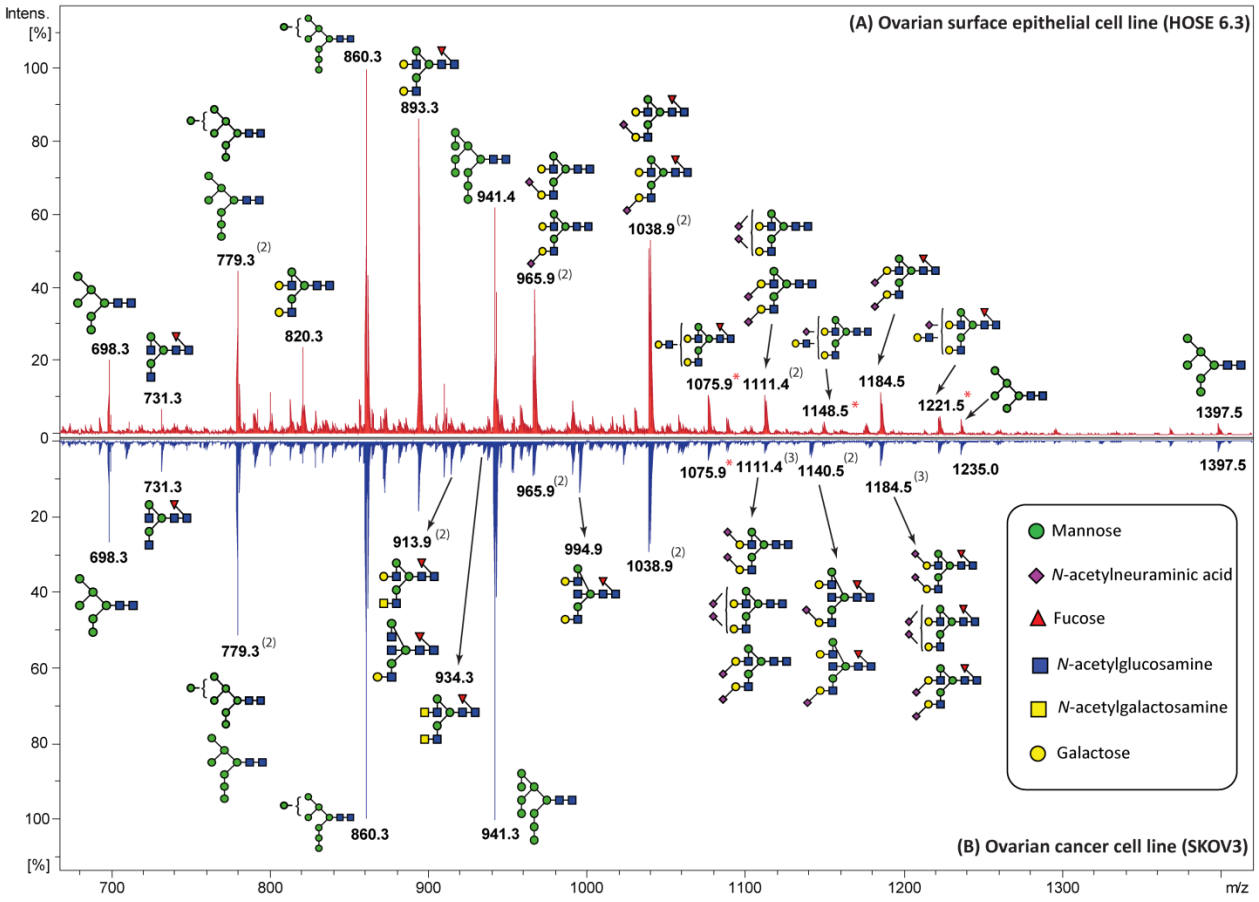
Intens.
[%]
(A) Ovarian surface epithelial cell line (HOSE 6.3)
(B) Ovarian cancer cell line (SKOV3)
m/z
Mannose
N-acetylneuraminic acid
Fucose
N-acetylglucosamine
N-acetylgalactosamine
Galactose

Figure 1

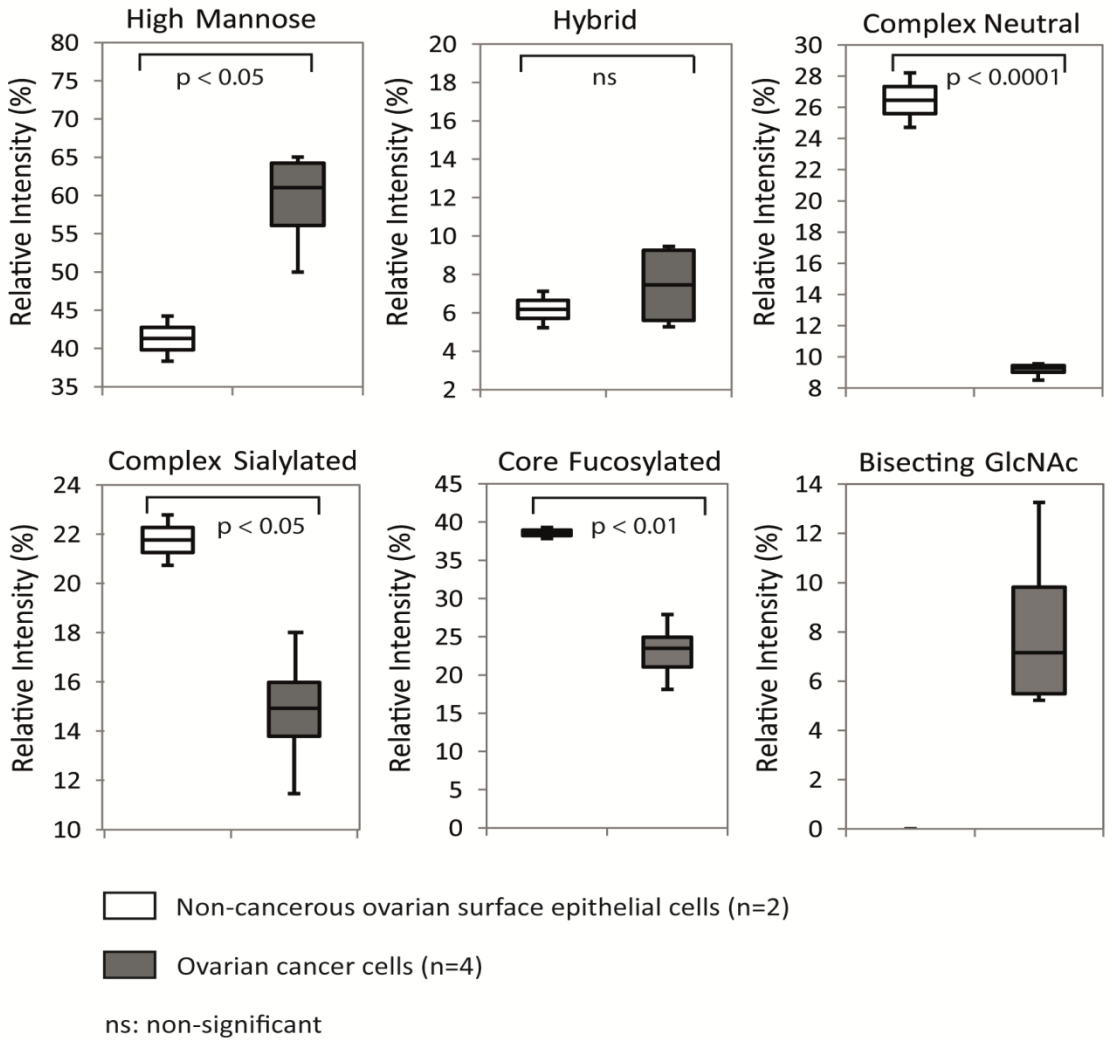
High Mannose
Relative Intensity (%)
p < 0.05
Hybrid
ns
Complex Neutral
p < 0.0001
Complex Sialylated
p < 0.05
Core Fucosylated
p < 0.01
Bisecting GlcNAc
Non-cancerous ovarian surface epithelial cells (n=2)
Ovarian cancer cells (n=4)
ns: non-significant

Figure 2

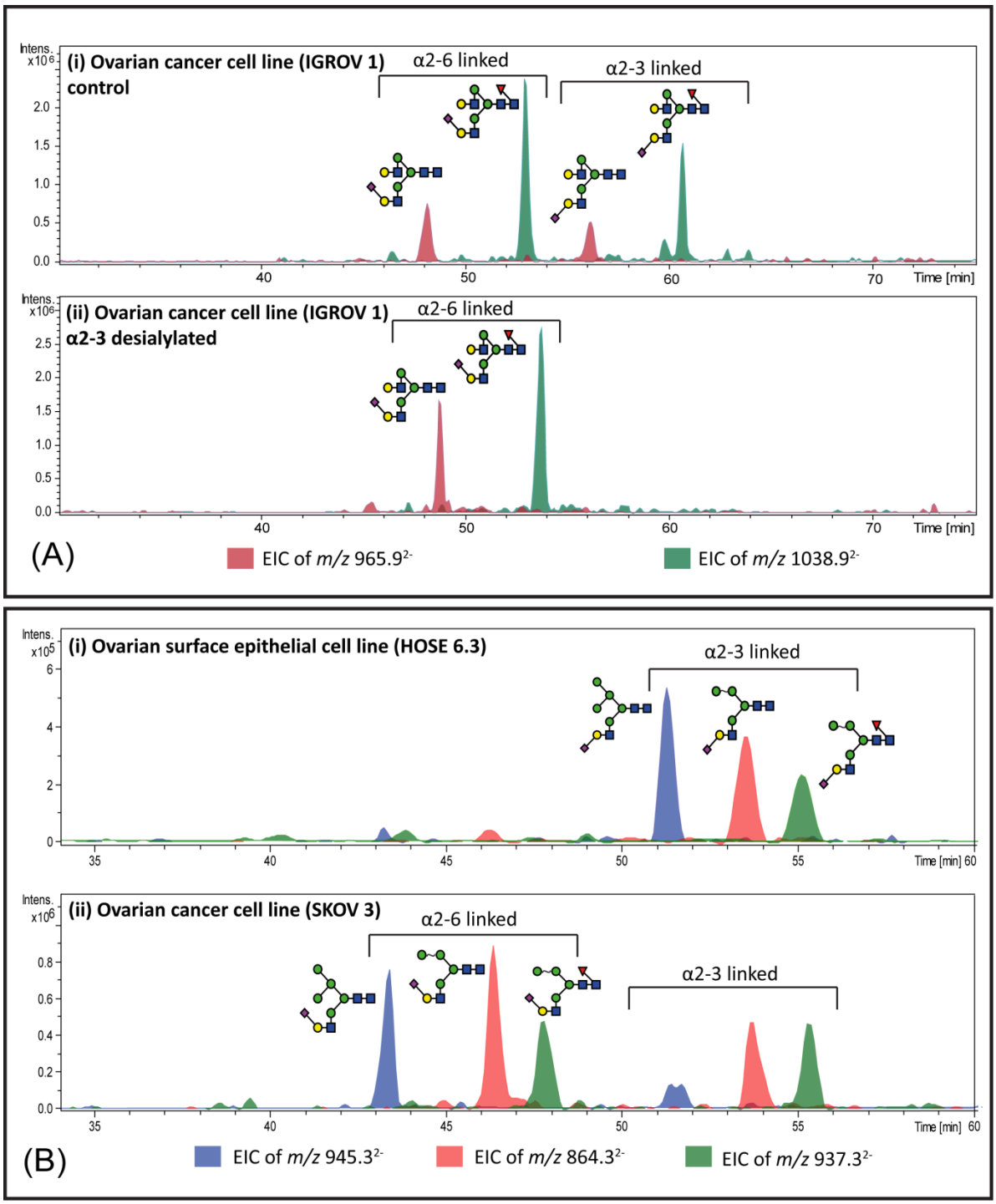
(i) Ovarian cancer cell line (IGROV 1) control
α2-6 linked
α2-3 linked
Intens. x10^6
Time [min]
(ii) Ovarian cancer cell line (IGROV 1) α2-3 desialylated
α2-6 linked
(A)
EIC of m/z 965.9^2-
EIC of m/z 1038.9^2-
(i) Ovarian surface epithelial cell line (HOSE 6.3)
α2-3 linked
Intens. x10^5
(ii) Ovarian cancer cell line (SKOV 3)
α2-6 linked
α2-3 linked
Intens. x10^6
(B)
EIC of m/z 945.3^2-
EIC of m/z 864.3^2-
EIC of m/z 937.3^2-

Figure 3

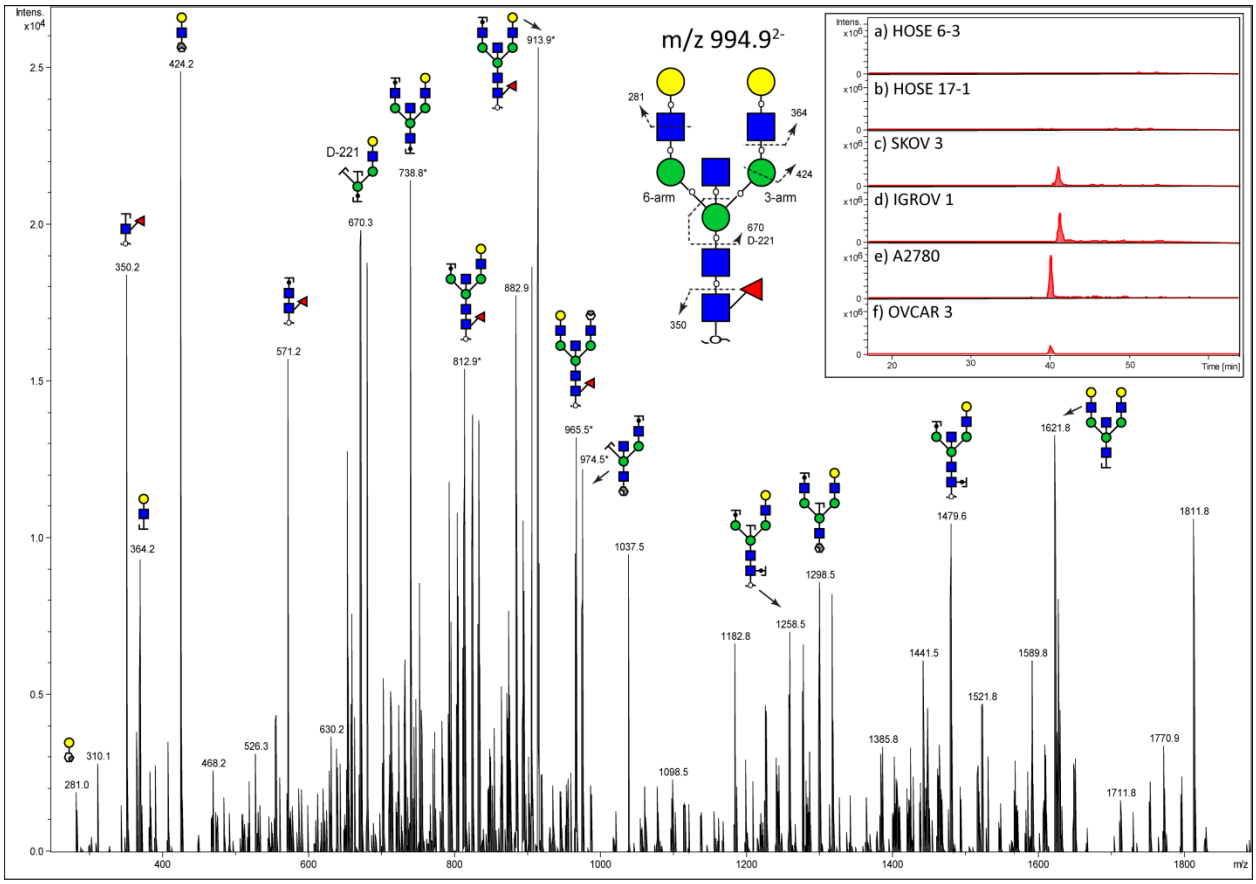
m/z 994.9 2-
6-arm
3-arm
281
364
424
670
D-221
350
a) HOSE 6-3
b) HOSE 17-1
c) SKOV 3
d) IGROV 1
e) A2780
f) OVCAR 3
Time [min]
Intens.
x10^4
m/z
424.2
913.9*
738.8*
670.3
D-221
350.2
571.2
812.9*
882.9
965.5*
974.5*
1037.5
364.2
1182.8
1258.5
1298.5
1479.6
1621.8
1811.8
1441.5
1589.8
1521.8
1385.8
1770.9
1711.8
1098.5
630.2
526.3
468.2
310.1
281.0

Figure 4

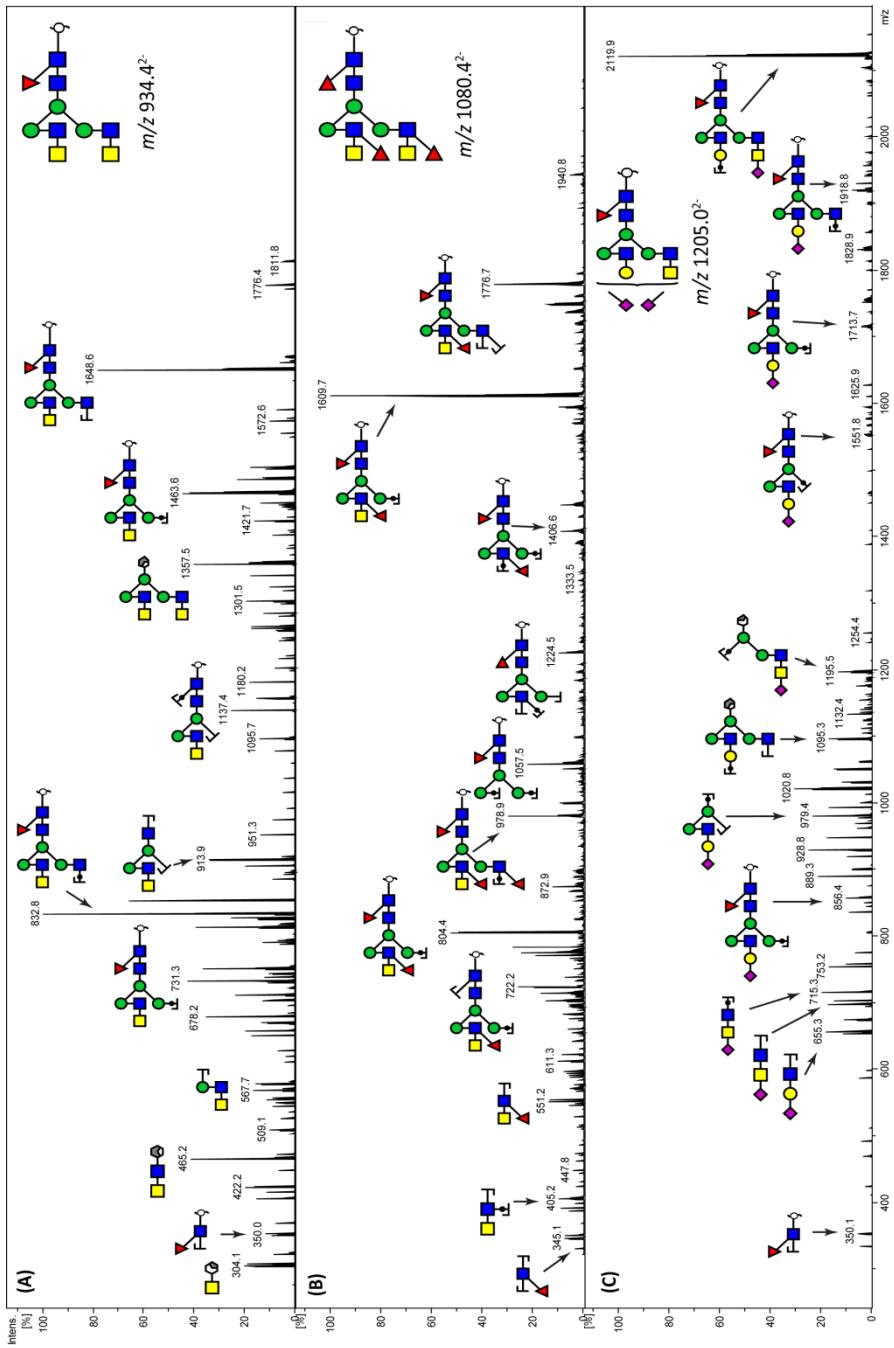

Figure 5

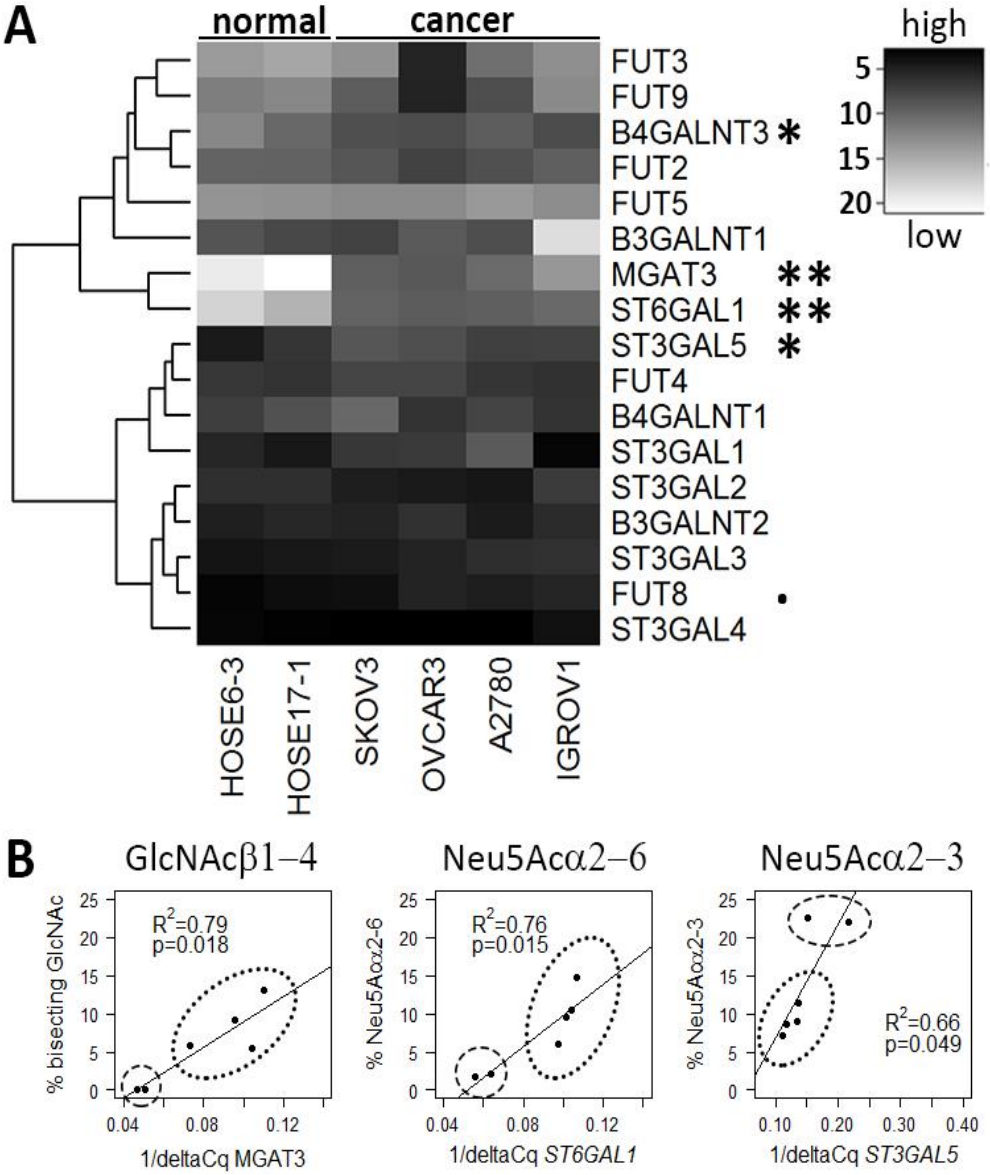
A
normal
cancer
high
5
10
15
20
low
FUT3
FUT9
B4GALNT3 *
FUT2
FUT5
B3GALNT1
MGAT3 **
ST6GAL1 **
ST3GAL5 *
FUT4
B4GALNT1
ST3GAL1
ST3GAL2
B3GALNT2
ST3GAL3
FUT8 •
ST3GAL4
HOSE6-3
HOSE17-1
SKOV3
OVCAR3
A2780
IGROV1
B
GlcNAcβ1–4
Neu5Acα2–6
Neu5Acα2–3
% bisecting GlcNAc
R2=0.79
p=0.018
1/deltaCq MGAT3
% Neu5Acα2-6
R2=0.76
p=0.015
1/deltaCq ST6GAL1
% Neu5Acα2-3
R2=0.66
p=0.049
1/deltaCq ST3GAL5

Figure 6

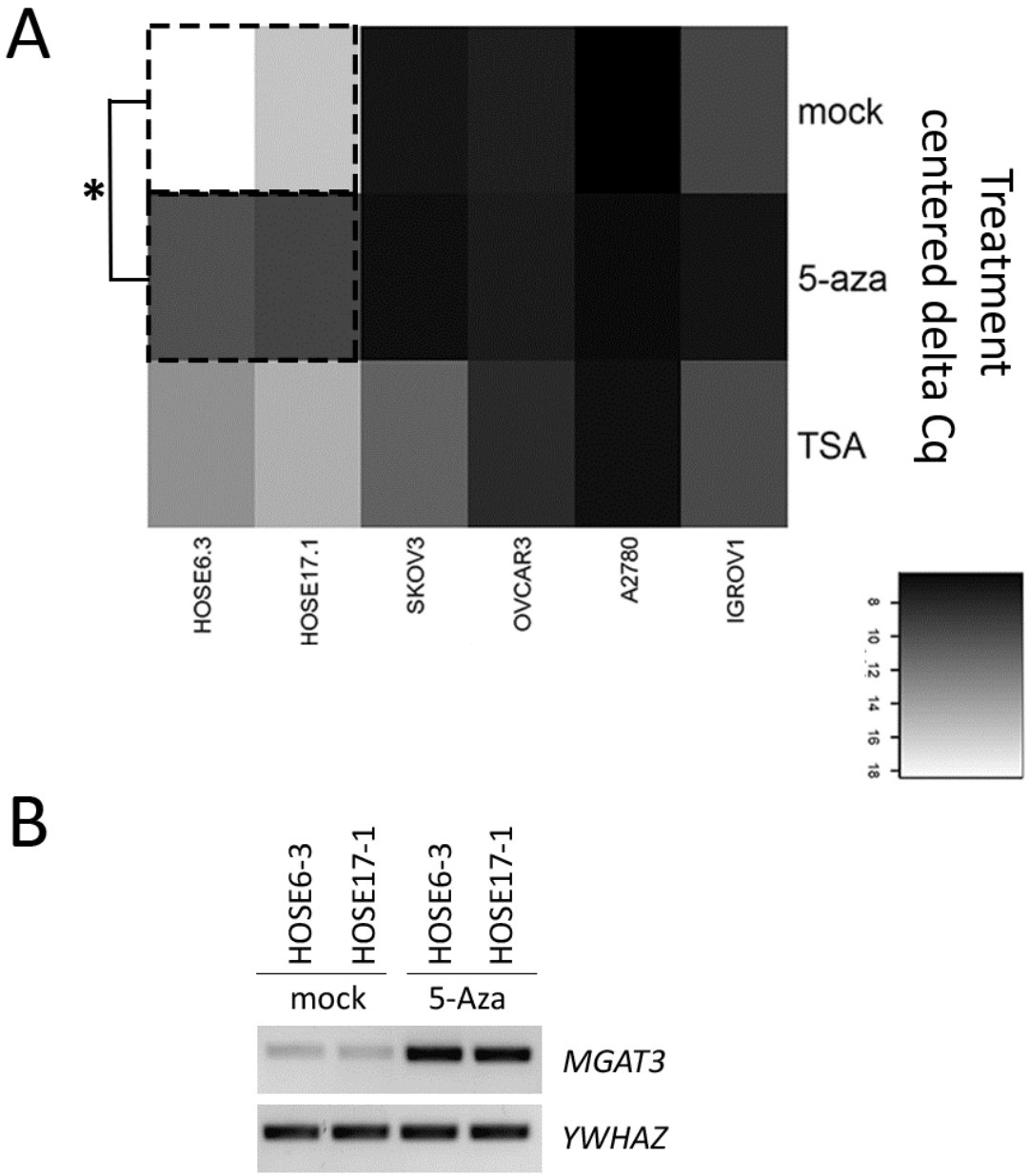
A
*
mock
5-aza
TSA
HOSE6.3
HOSE17.1
SKOV3
OVCAR3
A2780
IGROV1
Treatment
centered delta Cq
8
10
12
14
16
18
B
HOSE6-3
HOSE17-1
HOSE6-3
HOSE17-1
mock
5-Aza
MGAT3
YWHAZ

Figure 7